ChemPubSoc Europe

FULL PAPERS

Visualising cathepsins in tumours: Cysteine cathepsins are key players in tumour pathology. An azadipeptide nitrile with high affinity for cathepsins L, S, B, and K was labelled with fluorine-18 and investigated for its pharmacokinetic properties. PET imaging studies with tumour-bearing mice indicate the tumour accumulation of the probe and the potential of tumour targeting for this inhibitor class.

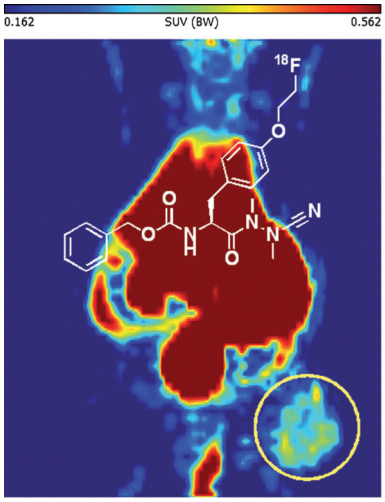

R. Löser, R. Bergmann, M. Frizler, B. Mosch, L. Dombrowski, M. Kuchar, J. Steinbach, M. Gütschow, J. Pietzsch*

■■ – ■■

Synthesis and Radiopharmacological Characterisation of a Fluorine-18-Labelled Azadipeptide Nitrile as a Potential PET Tracer for in vivo Imaging of Cysteine Cathepsins

DOI: 10.1002/cmdc.201300135

Synthesis and Radiopharmacological Characterisation of a Fluorine-18-Labelled Azadipeptide Nitrile as a Potential PET Tracer for in vivo Imaging of Cysteine Cathepsins

Reik Löser,*[a, c] Ralf Bergmann,[a] Maxim Frizler,[b] Birgit Mosch,[a] Lilli Dombrowski,[a] Manuela Kuchar,[a, c] Jörg Steinbach,[a, c] Michael Gütschow,[b] and Jens Pietzsch[a, c]

A fluorinated cathepsin inhibitor based on the azadipeptide nitrile chemotype was prepared and selected for positron emission tomography (PET) tracer development owing to its high affinity for the oncologically relevant cathepsins L, S, K and B. Labelling with fluorine-18 was accomplished in an efficient and reliable two-step, one-pot radiosynthesis by using 2-[^{18}F]fluoroethylnosylate as a prosthetic agent. The pharmacokinetic properties of the resulting radiotracer compound were studied in vitro, ex vivo and in vivo in normal rats by radiometabolite analysis and small-animal positron emission tomography. These investigations revealed rapid conjugate formation of the tracer with glutathione in the blood, which is associated with slow blood clearance. The potential of the developed ^{18}F-labelled probe to image tumour-associated cathepsin activity was investigated by dynamic small-animal PET imaging in nude mice bearing tumours derived from the human NCI-H292 lung carcinoma cell line. Computational analysis of the obtained image data indicated the time-dependent accumulation of the radiotracer in the tumours. The expression of the target enzymes in the tumours was confirmed by immunohistochemistry with specific antibodies. This indicates that azadipeptide nitriles have the potential to target thiol-dependent cathepsins in vivo despite their disadvantageous pharmacokinetics.

Introduction

The huge and diverse class of proteolytic enzymes accounts for 2% of the human genome and plays a pivotal role in the pathophysiology of tumours. Proteases of all mechanistic subclasses (Ser/Thr-, Cys-, Asp- and metalloproteases) have been discussed to be involved in the extensive network of proteolysis leading to tumour invasion and metastasis.[1] A prominent function in enabling tumour cells for metastasis has been assigned to matrix-metalloproteinases (MMPs).[2] Beside these enzymes, the thiol-dependent cathepsins are attracting increasing interest in tumour biology as key players in tumour-linked proteolysis. Eleven different representatives of these papain-like cysteine proteases are encoded in the human genome and the expressed enzymes are localised inside the lysosome under usual conditions.[3] The most significant role of these proteases in tumour progression has become evident for cathepsins L, B and S.[4] Their particular function in tumour progression is mainly exerted by the extracellular action of the secreted proteases on proteins that are important either for the interaction of tumour cells with their microenvironment or for the interaction of tumour cells with neighbouring tumour cells.[5] In detail, cathepsins are able to degrade the components of both the basement membrane and the extracellular matrix.[6] Furthermore, they have the capability for proteolytic activation of alternative proteases participating in this process, such as MMP-1 and MMP-3, as well as the serine protease urokinase plasminogen activator (uPA), from their respective zymogens.[6] The increased cathepsin activity in tumours does not only originate from tumour cells but also from tumour-associated benign cells, such as macrophages and other immune cells, endothelial cells and fibroblasts.[5a] Tumour cells and endothelial cells mainly contribute the cathepsins L and B, whereas the cathepsin activity of tumour-associated immune cells is dominated by cathepsin S. It has been shown in numerous studies that increased cathepsin activity is correlated with the invasive potential and, thus, the malignancy of tumour cells.[7] A correlation of elevated cathepsin B activity with malignancy was evidenced for various tumour entities, such as melanoma,[8] glioma[9] and breast cancer.[10] Cathepsin L has been shown to be crucial for the invasive capacity of oncogenically transformed fibroblasts[11] and is involved in the metastasis of melanoma cells.[12] The connection of cathepsin S activity in tumours to increased malignancy seems to be less evident than that for the cathepsins B and L. Nevertheless, cathepsin S is im-

[a] Dr. R. Löser, Dr. R. Bergmann, Dr. B. Mosch, L. Dombrowski, M. Kuchar, Prof. Dr. J. Steinbach, Prof. Dr. J. Pietzsch
Institut für Radiopharmazeutische Krebsforschung
Helmholtz-Zentrum Dresden-Rossendorf
Bautzner Landstraße 400, 01328 Dresden (Germany)
E-mail: r.loeser@hzdr.de

[b] Dr. M. Frizler, Prof. Dr. M. Gütschow
Pharmazeutisches Institut, Pharmazeutische Chemie I
Rheinische Friedrich-Wilhelms-Universität
An der Immenburg 4, 53121 Bonn (Germany)

[c] Dr. R. Löser, M. Kuchar, Prof. Dr. J. Steinbach, Prof. Dr. J. Pietzsch
Fachrichtung Chemie und Lebensmittelchemie
Technische Universität Dresden
Bergstraße 66c, 01062 Dresden (Germany)

Supporting information for this article is available on the WWW under http://dx.doi.org/10.1002/cmdc.201300135.

portant for tumour pathology. Concerning its prognostic value, contradictory findings have been reported. In lung cancer, increased activity of the enzyme was correlated with a better prognosis,[13] whereas recurrence-free survival was decreased for patients with colorectal carcinoma overexpressing cathepsin S.[14] In accordance with the latter result, the activity of this protease was found to be lower in glioblastoma stem cells than in their invasive progenitors.[15]

The function of cathepsin K in neoplastic conditions is less well understood than that of the enzymes mentioned above. It is one of the most potent matrix-degrading enzymes known[16] and its expression mainly occurs in osteoclasts[17] but is not restricted to these cells. Cathepsin K could be detected in various prostate cancers, with higher levels in metastatic than in primary tumour cells.[18] Immunoreactivity against cathepsin K was shown to be associated with the increased invasive potential of lung carcinoma.[19] In addition, breast-tumour-associated stromal fibroblasts were found to be cathepsin K positive and able to stimulate the invasion of breast-tumour epithelial cells in vitro.[20]

Due to the evident importance of thiol-dependent cathepsins for tumour biology, several efforts have been undertaken towards the development of molecular probes that are capable of imaging the activity of these enzymes in vivo but also of unraveling their functions in cell-based experiments.[21]

Cy5.5-conjugated methoxypoly(ethylene glycol)-grafted poly-L-lysines were found to be useful agents for optical imaging of cathepsin B in vivo. Multiple fluorophore units were linked to the polymer backbone, which led to internal quenching of the near-infrared fluorescence (NIRF). Unmodified lysines within the polymer served as recognition sites for cathepsin B-catalysed cleavage, which led to an enhanced fluorescence signal. This NIRF probe was used for the imaging of human breast cancers implanted in nude mice and a correlation was found with cathepsin B activity.[22] Besides substrate-based probes, fluorescently labelled inhibitors containing an acyloxymethylketone substructure were successfully developed for in vivo application.[23] For application in vivo, optical imaging has severe limitations in sensitivity and penetration depth and is excelled by molecular imaging based on radiolabelled probes in these regards. Cathepsin-inhibiting peptide-derived diazoketones and epoxides have been labelled with iodine-125 and used for cell-based in vitro studies but reports on their in vivo behaviour are missing.[24]

Positron emission tomography (PET) represents the most favourable modality for functional imaging in terms of sensitivity, quantitative image evaluation and penetration depth.[25] For example, successful attempts have already been made to image MMPs with radiofluorinated inhibitors.[26] The development of cathepsin-targeting molecular probes labelled with positron-emitting radionuclides has started only very recently with copper-64-labelled acyloxymethylketones.[27] Among the various radionuclides available for PET imaging, fluorine-18 can be considered as optimal because it has a high content of positron emission (97%) and an intermediate half-life of 109.8 min. Moreover, fluorine atoms can form highly stable covalent bonds with carbon atoms. For these reasons, fluorine-18 represents the radionuclide of choice to develop PET tracers based on small molecules.[28] The aim of this study was the design and synthesis of a fluorine-containing cathepsin inhibitor and its labelling with fluorine-18, as well as its characterisation in vivo.

Peptidic and non-peptidic compounds containing cyano groups have been comprehensively explored as inhibitors for thiol-dependent cathepsins in recent years.[29] Among this class of inhibitors, azadipeptide nitriles have proven advantageous due to their high potency, combined with notable stability towards degradation by serine proteases.[30] Extensive structure–activity relationships have been deduced for these compounds[31] and their efficiency for targeting papain-like cysteine proteases in cellular systems has been established.[32] Therefore, this inhibitor chemotype was selected to develop a PET tracer for visualisation of cysteine cathepsins in vivo.

Results and Discussion

Synthesis of the non-radioactive reference compound and enzyme inhibitory activity

The azadipeptide nitrile **1** was prepared as described recently.[31a] Compound **1** was O-alkylated by using 1-bromo-2-fluoroethane (**2**), which in turn was prepared by a published method.[33] This furnished the fluorine-containing azadipeptide nitrile **3** (Scheme 1), which served as a non-radioactive reference compound of the desired tracer.

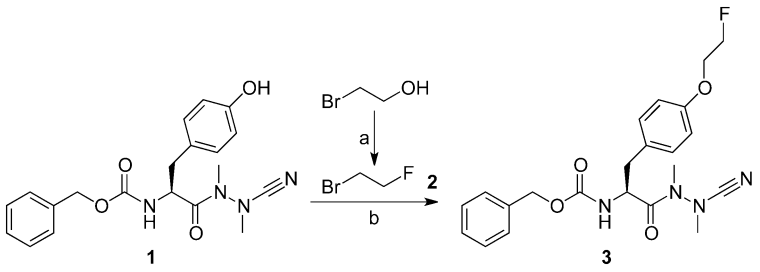

Scheme 1. Synthesis of the fluorine-containing azadipeptide nitrile **3**. *Reagents and conditions*: a) DAST, CH_2Cl_2, −50 °C→RT; b) NaH, DMF. DAST = diethylaminosulfur trifluoride; DMF = *N*,*N*-dimethylformamide.

Azadipeptide nitriles have been found to be highly potent slow-binding inhibitors of papain-like cysteine proteases.[30,31] The inhibitory activity of **1** towards the oncologically important cathepsins L, S, B and K was reported to be in the sub-nanomolar range (Table 1).[31a] The inhibition constants, K_i, as well as the rate constants, k_{on} and k_{off}, of the fluorine-containing azadipeptide nitrile **3** were determined in kinetic enzyme assays for cathepsins L, S, B and K. Similarly to those of the parent compound **1**, the inhibition constants of the fluoroethyl derivative **3** were in the sub-nanomolar range, with the exception of those for cathepsin B. The lower binding affinity of **3** relative

Table 1. Inhibition of thiol-dependent cathepsins by the azadipeptide nitriles **1** and **3**.[a]

Compd	Cathepsin L			Cathepsin S			Cathepsin B			Cathepsin K		
	K_i [nM]	k_{on} [10^3 M^{-1} s^{-1}]	k_{off} [10^{-3} s^{-1}]	K_i [nM]	k_{on} [10^3 M^{-1} s^{-1}]	k_{off} [10^{-3} s^{-1}]	K_i [nM]	k_{on} [10^3 M^{-1} s^{-1}]	k_{off} [10^{-3} s^{-1}]	K_i [nM]	k_{on} [10^3 M^{-1} s^{-1}]	k_{off} [10^{-3} s^{-1}]
1[b]	0.36 ± 0.03	4200 ± 100	1.5 ± 0.1	0.86 ± 0.02	500 ± 30	0.43 ± 0.03	0.38 ± 0.03	79 ± 22	0.030 ± 0.009	0.16 ± 0.01	320 ± 20	0.051 ± 0.005
3	0.73 ± 0.06	930 ± 100	0.68 ± 0.09	0.79 ± 0.06	560 ± 100	0.44 ± 0.09	2.4 ± 0.1	190 ± 10	0.46 ± 0.03	0.17 ± 0.01	210 ± 50	0.036 ± 0.009

[a] Data represent the mean ± SEM; experiments were performed in duplicate with at least five different inhibitor concentrations. [b] Values taken from Ref. [31a].

to **1** towards cathepsin B can be attributed to a notably increased first-order rate constant, k_{off}, to describe the decay of the enzyme–inhibitor complex, whereas the second-order rate constant for the association to the complex, k_{on}, was slightly higher than that of the parent compound **1**. Owing to its high affinity for the oncologically important thiol-dependent cathepsins, **3** was used as a basis to develop a PET tracer targeting these enzymes.

Synthesis of labelling precursors and radiolabelling

In analogy to the synthesis of the non-radioactive reference **3**, ^{18}F-fluoroethylation of **1** appeared to be a promising strategy to afford the radiolabelled azadipeptide nitrile [^{18}F]**3**. As radiolabelling by ^{18}F-fluoroethylation is commonly performed by employing 2-[^{18}F]fluoroethyltosylate,[34] initial efforts towards the preparation of [^{18}F]**3** focused on the conversion of **1** with this alkylating agent. A two-step, one-pot strategy was followed, which consisted of the reaction of commercially available ethylene glycol-1,2-ditosylate (**5a**) with [^{18}F]fluoride to form 2-[^{18}F]fluoroethyltosylate ([^{18}F]**6a**), which was converted without isolation, with **1** used in a slight excess over **5a** (Scheme 2). Analysis by radio-TLC indicated the formation of [^{18}F]**3** in acetonitrile at 100 °C. However, the labelling yields were low and a considerable amount of the ^{18}F activity remained in the intermediate 2-[^{18}F]fluoroethyltosylate ([^{18}F]**6a**; see table S1 in the Supporting Information). An increase in the temperature to 115 °C resulted in higher yields of the desired product, which, however, did not exceed 26%. The amount of [^{18}F]**6a** continuously decreased with the reaction time. This decline was not accompanied by an increase in [^{18}F]**3** in the same manner, which indicated the decomposition of [^{18}F]**6a** under these reaction conditions. The degradation of the ^{18}F-fluoroethylation agent was even more pronounced in DMF at 90 °C and only traces of [^{18}F]**6a** and [^{18}F]**3** could be detected at 150 °C with this solvent.

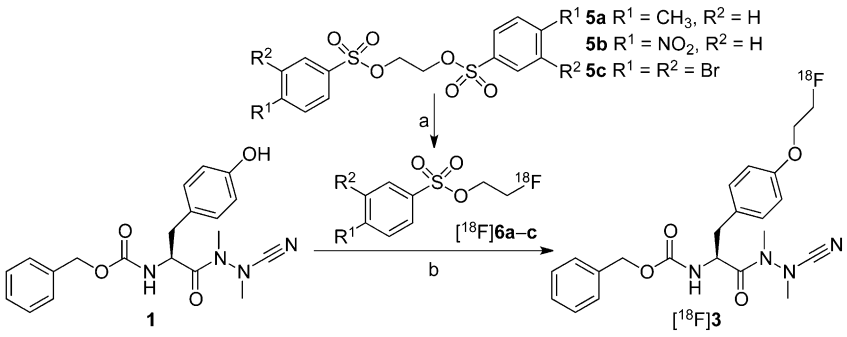

Scheme 2. Two-step, one-pot radiosynthesis of [^{18}F]**3**. *Reagents and conditions*: a) [^{18}F]KF, K_2CO_3, K222, CH_3CN, 90 °C, 5 min; b) reaction solution from (a), 1 M Cs_2CO_3/H_2O, 115 °C, 10 min. K222 = Kryptofix 222.

The isolation of the labelled azadipeptide nitrile [^{18}F]**3** was attempted for the most favourable conditions (acetonitrile as the solvent, 115 °C, 20 min reaction time) by semi-preparative reversed-phase (RP) HPLC. This resulted in [^{18}F]**3** of poor radiochemical purity (RCP) because the separation from the remaining [^{18}F]**6a** proved difficult. The low labelling yields and the difficult separation of [^{18}F]**3** from [^{18}F]**6a** led to the use of alternative 2-[^{18}F]fluoroethylbenzenesulfonates being envisaged. The selection of the benzenesulfonate leaving groups was inspired by the study of Musachio et al.[35] The required ethylene glycol-1,2-dibenzenesulfonates **6b** and **6c** were prepared by following published procedures (see scheme S1 in the Supporting Information).

The reaction of ethylene glycol-1,2-dinosylate (**5b**) with [^{18}F]fluoride was optimised with regard to the amount of precursor and reaction time. The highest labelling yields of [^{18}F]**6b** were achieved with 3 and 5 mg of **5b** in acetonitrile. Conversion of [^{18}F]**6b** with **1** resulted in the formation of [^{18}F]**3** in an analytical radiochemical yield (determined by radio-TLC; see figure S2 in the Supporting Information) of 74% after 10 min in acetonitrile at 115 °C (Table 2). More reproducible results could be obtained when 5 mg of **5b** were used instead of 3 mg. Radiofluorination of ethylene glycol-1,2-bis(3,4-dibromobenzenesulfonate) (**5c**) proceeded with a lower analytical radiochemical yield than those with **5a** and **5b** and the results for ^{18}F-fluoroethylation with [^{18}F]**6c** were even less beneficial than with the corresponding tosylate (Table 2).

Besides the two-step, one-pot approach for ^{18}F-labelling of **3**, direct radiofluorination was also considered. Hence, the corresponding tosylate and nosylate precursors **7a** and **7b** were prepared by treating **1** with an excess of **5a** and **5b**, respectively, as described for other compounds (Scheme 3).[36] The precursors **7a** and **7b** were treated with [^{18}F]fluoride as detailed in the Experimental Section. Under favourable conditions (3 mg of precursor, 5 min reaction

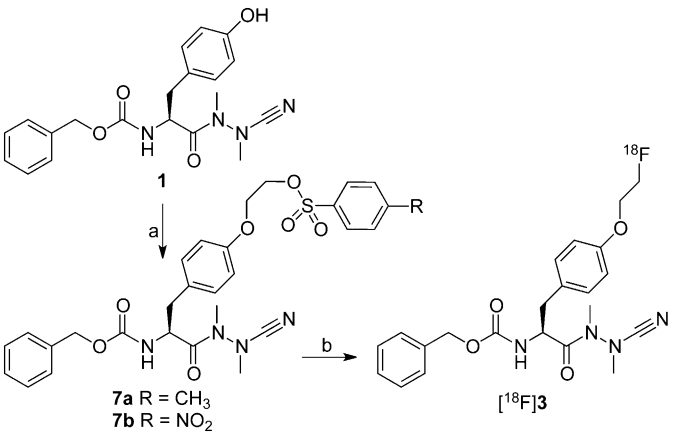

Scheme 3. Synthesis of direct-labelling precursors **7a** and **7b** and one-step radiolabelling of [^{18}F]**3**. *Reagents and conditions*: a) **5a** or **5b**, respectively, K_2CO_3, CH_3CN, reflux; b) [^{18}F]KF, K_2CO_3, K222, CH_3CN, 90 °C.

Table 2. Yields and conditions for the radiosynthesis of [^{18}F]**3** by ^{18}F-fluoroethylation of **1** with 2-[^{18}F]fluoroethylnosylate ([^{18}F]**6b**) and 2-[^{18}F]fluoroethyl-3,4-dibromobenzenesulfonate ([^{18}F]**6c**).

Radiofluorination precursor	$t_{reaction}$ [min]	Analytical radiochemical yield [%][a]	
		[^{18}F]**6b/c**	[^{18}F]**3**
5b	5	31	58
5b	10	6	74
5b	20	0	49
5c	5	7	30
5c	10	3	29
5c	20	0	22

[a] Determined by radio-TLC.

time), [^{18}F]**3** was formed from the nosylate **7b** with an analytical radiochemical yield of 12%, whereas no product formation could be observed with the corresponding tosylate **7a** (see table S2 and figure S2 in the Supporting Information). Therefore, it was concluded that direct labelling is less advantageous than ^{18}F-fluoroethylation and the preparative radiosynthesis of [^{18}F]**3** was optimised for the two-step, one-pot procedure with 2-[^{18}F]fluoroethylnosylate ([^{18}F]**6b**) as the alkylating agent. This led to a reliable procedure for the preparation of [^{18}F]**3** with an average radiochemical yield after isolation of (26.3 ± 4.6)% (n = 13), with a synthesis time of 140 min by starting with drying of the [^{18}F]fluoride. The radiochemical purities were greater than 98% and the specific activities ranged from 2.9–30.4 GBq μmol^{-1} (see figure S3 and S4 in the Supporting Information for the chromatograms).

Immunohistochemical detection of cathepsins in xenografted NCI-H292 tumours

The overexpression of cathepsins L and B in lung carcinoma has been reported in several studies.[37] Therefore, we decided to use tumour xenografts derived from the human pulmonary mucoepidermoid carcinoma cell line NCI-H292 in nude mice as a model to investigate the potential of fluorine-18-labelled azadipeptide nitrile [^{18}F]**3** for imaging the cathepsin activity in tumours.

The expression of cathepsins L, S, B and K was analysed in selected mouse and rat organs and in tumour xenografts by using immunohistochemical staining. Representative images of mouse specimens and tumour xenografts are shown in Figure 1 and the corresponding negative controls (staining without primary antibodies) can be found in the Supporting Information (figure S5). In tumour xenografts, all four cathepsins were detected with higher intensity for cathepsins L and K than for cathepsins S and B. The skeletal muscle was chosen as an internal negative control. It is of note that cathepsin L expression was detectable in mouse but not in rat muscle. Cathepsins S, B and K showed a signal in neither mouse nor rat muscle. In the liver, all cathepsins could be detected, although cathepsins B and K had very low levels in the mouse liver. The spleen showed strong expression of all cathepsins, with the exception of cathepsin B in the rat, for which no specific signal was detectable (data not shown in detail). A likewise intensive cathepsin staining was observed in the kidney, with the exception of weak signals for cathepsin B in the mouse and cathepsin K in the rat. Taken together, we detected considerable ex-

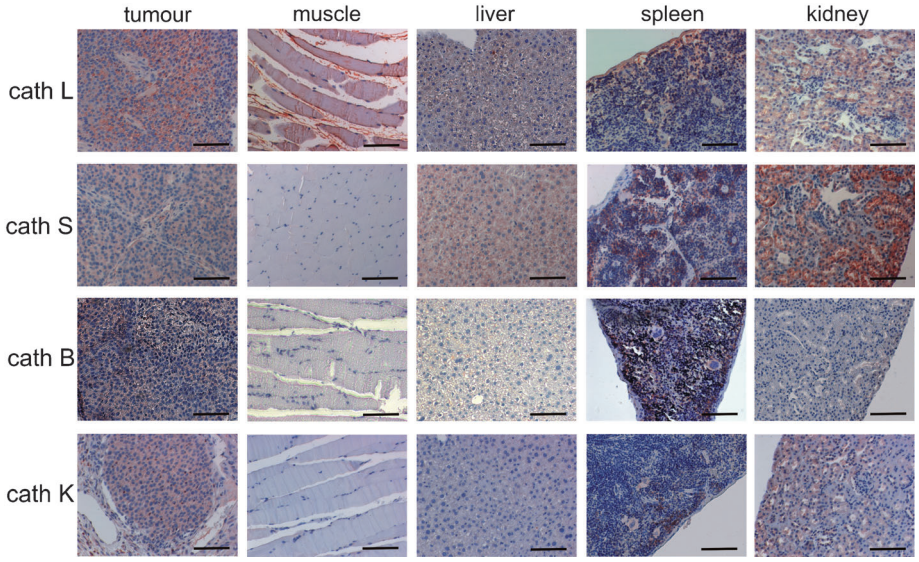

Figure 1. Immunohistochemical detection of cathepsins in NCI-H292 tumour xenografts and mouse organs (skeletal muscle, liver, spleen, kidney). Tissue pieces were paraffin-embedded, sliced into 5 μm sections and stained as described in the Experimental Section. Red colour indicates cathepsin staining; blue colour displays cell nuclei (counterstaining with Mayer's Hematoxylin). Bar = 100 μm; cath = cathepsin.

pression of cathepsins L, S, B and K in rodent liver, spleen and kidney samples, as well as in the tumour xenografts. Thus, the NCI-H292 tumour xenografts were chosen as a promising model for radiopharmacological characterisation of [^{18}F]**3** as a tumour-imaging agent.

Radiopharmacological characterisation in vitro, ex vivo and in vivo

Log P *and in vitro stability*

A log *P* value of 2.3 was determined for [^{18}F]**3** by the shaking-flask method.[38] The radiotracer will neither be protonated nor deprotonated in the physiological pH range. Probe [^{18}F]**3** was proven to be stable in phosphate-buffered saline (PBS) over 6 h at pH 7.4 (see figure S6 in the Supporting Information). Incubation of [^{18}F]**3** in rat blood plasma and fresh whole blood was carried out to model the behaviour of the compound in biological media without the interaction with the endothelium and the tissues in the organism. To a minor extent, [^{18}F]**3** was converted into a compound represented by a second peak with a lower retention time upon incubation in rat blood plasma. Analysis of the compound's fate in whole rat blood by radio-HPLC indicated its rapid transformation into more hydrophilic metabolites (see chromatogram for 0 min in Figure 2). Furthermore, determination of the distribution of the ^{18}F activity over the blood components revealed that 94% were accumulated immediately in the erythrocytes (Table 3). However, there are no cathepsins located in red blood cells; therefore, the accumulation in the erythrocytes must be driven by other mechanisms. Several drug molecules are known to accumulate in the erythrocytes by reversible binding to proteins or to undergo transformation inside these cells. Their penetration of the red-blood-cell membrane seems to be facilitated by aquaporins.[39] As cyanamides are known to react spontaneously with thiols,[40] it was assumed that the glutathione (GSH) conjugate

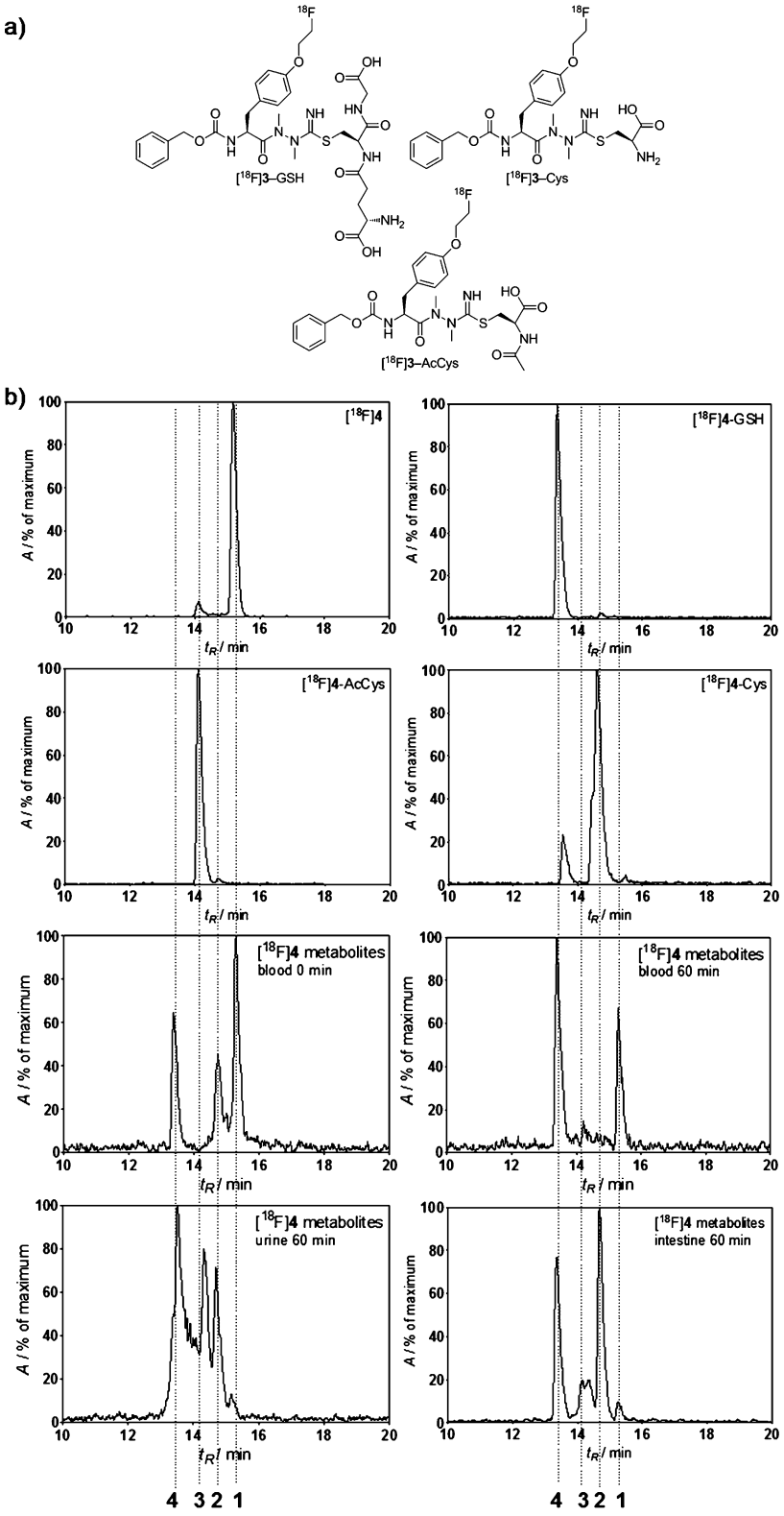

Figure 2. a) Structures of conjugates of [^{18}F]**3** with different endogenous cysteine derivatives. b) Radio-HPLC chromatograms of [^{18}F]**3**, [^{18}F]**3**–GSH, [^{18}F]**3**–AcCys, [^{18}F]**3**–Cys (obtained by incubation of [^{18}F]**3** with the corresponding cysteine derivatives) and metabolites of [^{18}F]**3** detected in rat blood, urine and intestine (0 min: blood in vitro; 60 min p.i.: blood, urine and intestine ex vivo, respectively).

Table 3. ^{18}F activity (% of blood activity) in the erythrocytes in vitro and ex vivo.

	in vitro			ex vivo		
time [min]	3	30	60	3	30	60
number of values	3	2	2	5	5	5
25th percentile	93.0	81.0	65.0	18.0	30.5	44.0
median	94.0	82.5	69.5	20.0	34.0	54.0
75th percentile	96.0	84.0	74.0	59.0	65.5	65.5

of [^{18}F]**3** was formed and resulted in temporary trapping inside the erythrocytes. To prove this, the radiotracer was incubated with 10 mM glutathione in PBS, a concentration that is similar to the glutathione level in erythrocytes.[41] Analysis by radio-HPLC confirmed the identity of the observed metabolite in rat blood with the product formed upon incubation with glutathione (Figure 2). To suppress this early metabolism of the radiotracer, attempts to lower the blood glutathione level were undertaken. Buthionine sulfoximine (BSO), a mechanism-based inhibitor of γ-glutamylcysteine synthetase,[42] the enzyme catalysing the first step of glutathione biosynthesis, has been used to systemically decrease the glutathione level in vivo.[43] With this aim, samples of rat blood were incubated with varying doses of BSO. Even in the presence of the highest dose of 3.75 mM, the metabolism of [^{18}F]**3** was not influenced. To sequester residual amounts of glutathione, blood samples were additionally incubated with varying doses of etacrynic acid, an antidiuretic agent, the pharmacological action of which relies on Michael adduct formation with cysteine.[44] Even the presence of both BSO and etacrynic acid, at concentrations of 3.53 and 2.94 mM, respectively, did not prevent the transformation of [^{18}F]**3** into the glutathione conjugate. Diethyl maleate, a stronger Michael acceptor than etacrynic acid, was also employed to sequester the glutathione of the blood.[45] Incubation of blood samples with 2% of this agent resulted in significant suppression of the radiotracer conversion (see figure S7 in the Supporting Information). This provides further evidence for the major metabolism of [^{18}F]**3** by reaction with glutathione. To prove this mechanism, erythrocyte ghosts were prepared and incubated with [^{18}F]**3**, whereupon no conversion of the radiotracer into the conjugate could be observed (see figure S8 in the Supporting Information). The conjugation of [^{18}F]**3** was also observed with cysteine to a minor extent in rat blood (Figure 2). The comparison of the ^{18}F-activity accumulation in the erythrocytes in vitro and in vivo revealed a fast uptake in the erythrocytes under both conditions (Table 3).

In vivo studies

Biodistribution and in vivo stability

The biodistribution of [^{18}F]**3** was studied in normal rats after 5 and 60 min post injection (p.i.). The ^{18}F-activity distribution data are shown both as a percentage of injected dose (%ID) in selected organs (Figure 3a) and as standardised uptake values (SUV_{bio}; Figure 3b).

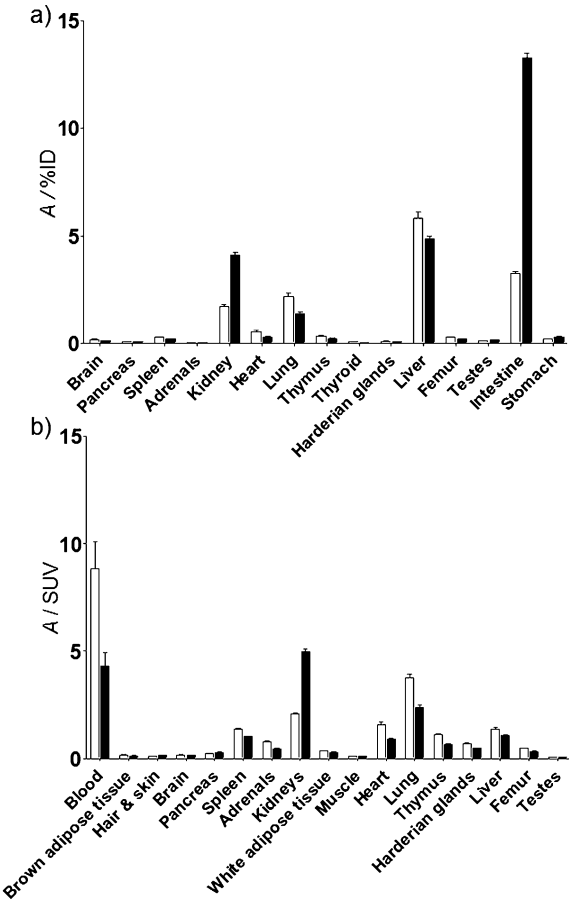

Figure 3. Biodistribution of [^{18}F]**3** in Wistar rats at 5 (□) and 60 min (■) after a single intravenous injection. a) Activity amount in selected organs (data are mean ± SD in %ID for 16 animals). b) Activity concentration (data are mean ± SD in SUV_{bio} for 16 animals).

Our data indicate that the majority of the ^{18}F activity after intravenous injection was eliminated through the kidneys. An amount of 41%ID was calculated for the urine after one hour. A minor part is eliminated through the hepatobiliary route. About 18%ID are accumulated in the liver and intestine after one hour. The ratio of approximately 2:1 between renal and hepatobiliary elimination can be explained by the conjugate formation between [^{18}F]**3** and glutathione leading to a considerably increased hydrophilicity, which favours renal filtration but also specific transport in the liver (see below).[46] Another large fraction of the ^{18}F activity is distributed in the whole organism (carcass), which might be explained by the high activity in the blood even after one hour. The clearance of the ^{18}F activity from the blood was relatively slow with a half-life of 39 min (Figure 4a); however, the metabolite-corrected [^{18}F]**3** clearance shows an even lower half-life of 114 min. An increase of the ^{18}F-activity concentration over time was only observed in the kidneys and resulted in an SUV of 4.98 ± 0.53 at 60 min p.i. The accumulation mechanism was not investigated in detail. The lung was a further organ with an SUV significantly greater than 1 after 60 min p.i., which probably can be attributed to the slow blood clearance of the ^{18}F activity.

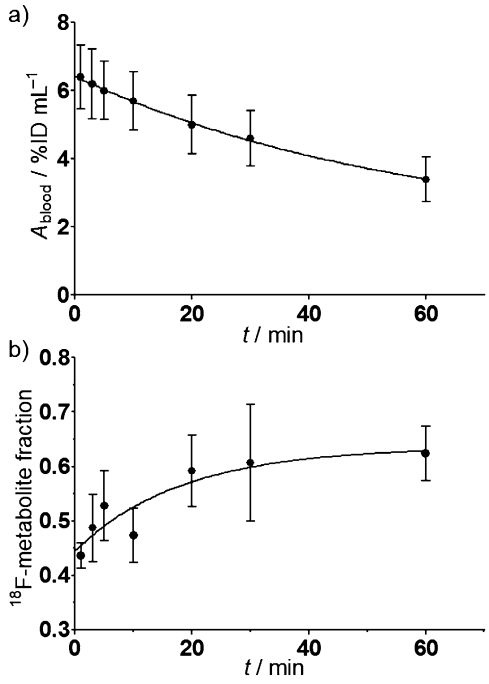

Figure 4. Ex vivo pharmacokinetics of the ^{18}F activity derived from compound [^{18}F]**3** distribution in the blood. a) ^{18}F-activity clearance in arterial blood of rats (mean ± SEM in %ID per mL of blood for 4 animals): $t_{1/2}$ = 39.3 min. b) Fraction of ^{18}F metabolites of the total activity in the arterial blood plasma.

The in vivo stability of [^{18}F]**3** was investigated in rat arterial blood samples. The overall blood volume of rats allows for collection of blood samples in amounts sufficient for radio-HPLC. The samples were collected at 1, 3, 5, 10, 20, 30 and 60 min p.i. Some of the radio-HPLC chromatograms are shown in Figure 2. Even though [^{18}F]**3** was synthesised with a very high RCP value of (98.5 ± 0.3)% (mean ± SEM for 23 syntheses), a small part was immediately hydrolysed to the free acid after dissolving [^{18}F]**3** in the injection electrolyte solution (E-153). The remaining RCP value of [^{18}F]**3** was (84 ± 3.5)% (mean ± SEM). The next step, incubation of [^{18}F]**3** with the first rat blood sample in vitro (designated as 0 s), revealed the immediate formation of metabolites. In the blood sample collected at one minute after injection, only 56% of the blood activity remained as original [^{18}F]**3** (see table S3 in the Supporting Information). The main metabolites were [^{18}F]**3**–GSH and [^{18}F]**3**–Cys. The [^{18}F]**3**–GSH was located in the erythrocytes, in which the ^{18}F activity increased from 30% of the total blood activity at 1 min to 55% after 60 min (Figure 5). Notably, despite vibrant conjugate formation, around 35% of original [^{18}F]**3** was still be detectable in the rat blood after one hour, as is evident from Figure 4b. Erythrocytes represent by far the most abundant cellular components of the blood, so the localisation of the radioactive metabolites inside these cells has great influence on the biodistribution and tissue-specific accumulation. An in vivo transport of glutathione conjugates inside rat erythrocytes and their elimination through the liver and bile into the intestine has also been reported for other xenobiotics.[46,47] This retention of the

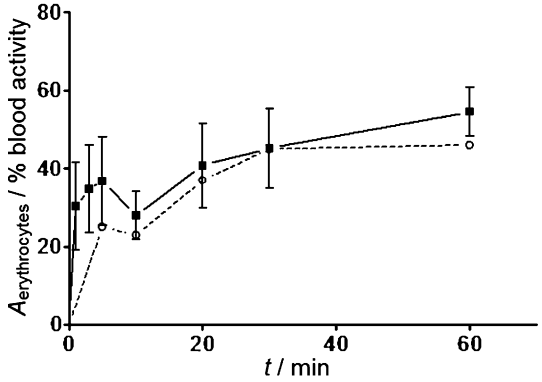

Figure 5. ^{18}F activity in the erythrocytes of arterial blood for five rats (■ mean ± SEM) and five mice (○ each data point: 1 mouse). The activity in the erythrocytes is expressed as % of activity in the whole blood sample.

activity in the red blood cells seems to be the reason for the low biological availability.

As mentioned above, ^{18}F-activity uptake in the erythrocytes in vitro is very fast and high (median 94.0%; decreased to 69.5% after one hour). Contrastingly, in vivo, the initial uptake after 3 min was only 20% (median) and increased to 54% after 60 min. This difference seems to be a result of the different reaction volume, as well as the resulting higher dilution in vivo and the continuous elimination of the radiolabelled compound and its metabolites from the plasma, which results in an increasing activity ratio in the erythrocytes to the plasma. A similar behaviour of [^{18}F]**3** was also observed in the blood of mice (Figure 5).

The urine and the content of the intestine were investigated by radio-HPLC 60 min after injection of [^{18}F]**3** into the rat.[^{18}F]**3** was also incubated with the respective biogenic thiols and, by comparison, [^{18}F]**3**–GSH and [^{18}F]**3**–Cys were identified as the main metabolites in the intestine. In contrast to this finding, the conjugate of [^{18}F]**3** and *N*-acetylcysteine (AcCys; mercapturic acid) appeared in considerable amounts in the urine, in addition to [^{18}F]**3**–Cys (Figure 2). In both the urine and the intestine, only negligible amounts of original [^{18}F]**3** were detectable. The formation of the conjugates derived from Cys and AcCys can be explained by peptidolytic processing of [^{18}F]**3**–GSH into [^{18}F]**3**–Cys followed by acetylation to form [^{18}F]**3**–AcCys mainly occurring in the liver but also in the epithelial cells of the proximal tubulus.[46]

Small-animal PET studies

The biodistribution and biokinetics of [^{18}F]**3** were also studied with small-animal PET in rats, NMRI mice and NMRI nude mice (nu/nu) bearing NCI-H292 tumour xenografts. The resulting images are depicted in Figure 6 (normal rat and normal mouse) and Figure 7 (tumour mouse) and confirm the data obtained for the ex vivo biodistribution of the compound. A large proportion of the activity was eliminated through the kidneys into the urine and through the hepatobiliary route into the intestine. The dynamics and metabolism of [^{18}F]**3** in mice seem to be faster than in rats (Figure 8). Hepatobiliary elimination of

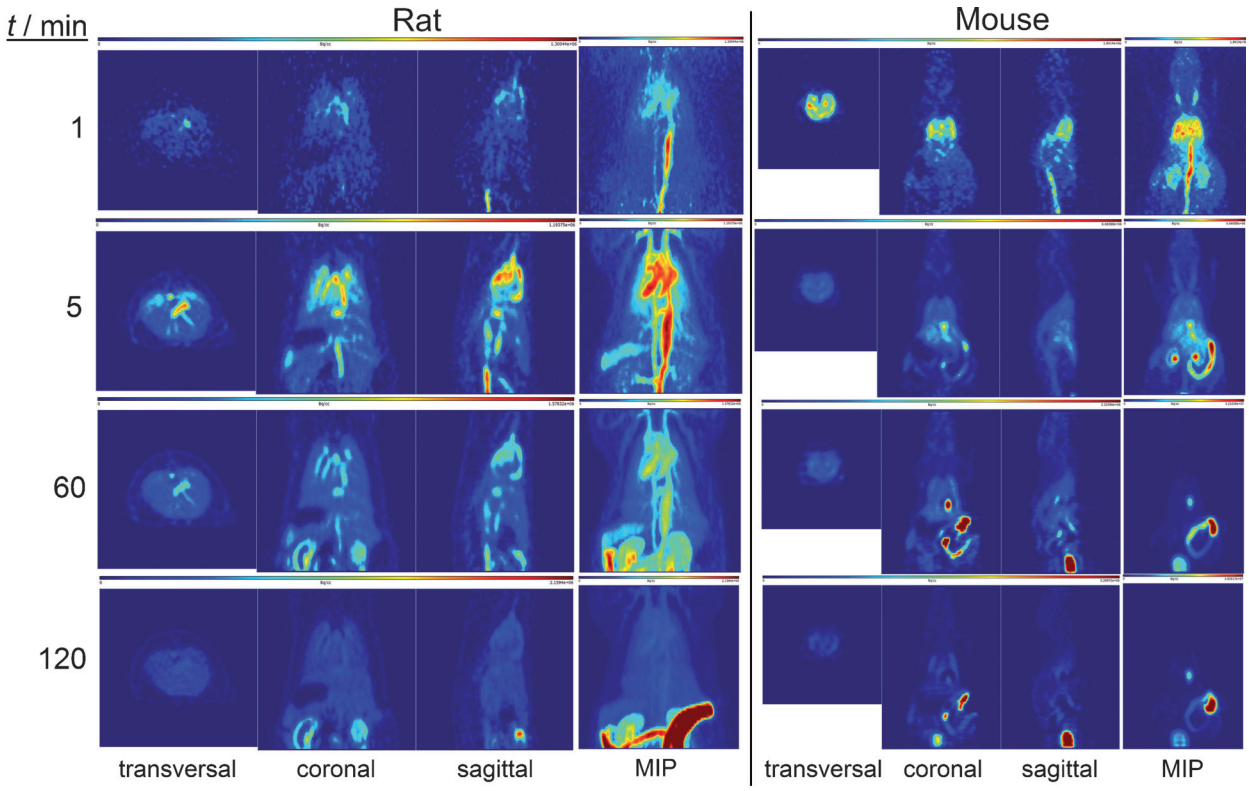

Figure 6. Representative small-animal PET images (transversal, coronal, sagittal planes and maximum intensity projection (MIP)) of [^{18}F]**3** in a Wistar rat and NMRI mouse after 1, 5, 60 and 120 min p.i., respectively.

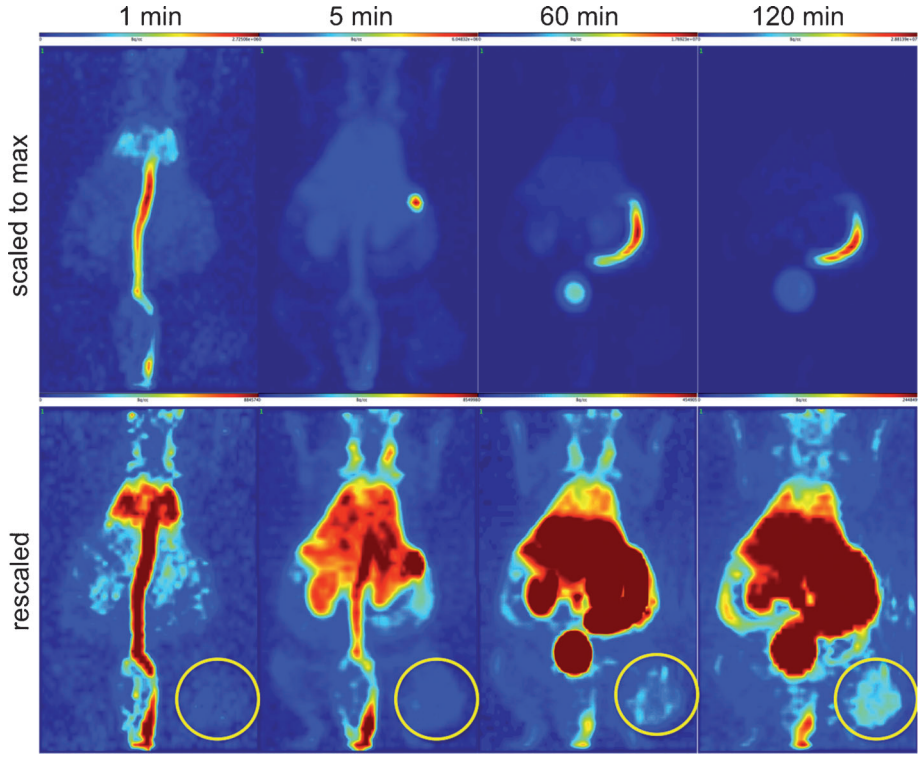

Figure 7. Maximum intensity projections of a representative PET study with a NCI-H292 tumour-bearing NMRI nu/nu mouse at 1, 5, 60 and 120 min after a single intravenous injection of [^{18}F]**3** (upper images are scaled to the maximum in the field of view; lower images are manually scaled; circle indicates the region of the tumour).

the compound was more pronounced in mice; about 40 %ID (calculated from the PET data) was in the gall bladder and the intestine after one hour. In the rat, only 3 %ID (calculated from the PET data) was in the intestine at the same time point (Figure 8 d). The blood clearance, as calculated from the PET data, was also substantially faster in the mice (half-life of 11.7 min; 95 % confidence interval: 6.7–45.4 min) than in the rats (30.9 min; 95 % confidence interval: 19.9–69.6 min). The faster hepatobiliary elimination rates observed in mice follow the general trend that excretion of xenobiotics proceeds faster in mice than in rats.[48]

Even after 2 h, the ^{18}F-activity concentration in the blood of the mice was high enough to visualise parts of the vascular system. After rescaling of the images, the tumour was clearly visible too (Figure 7). However,

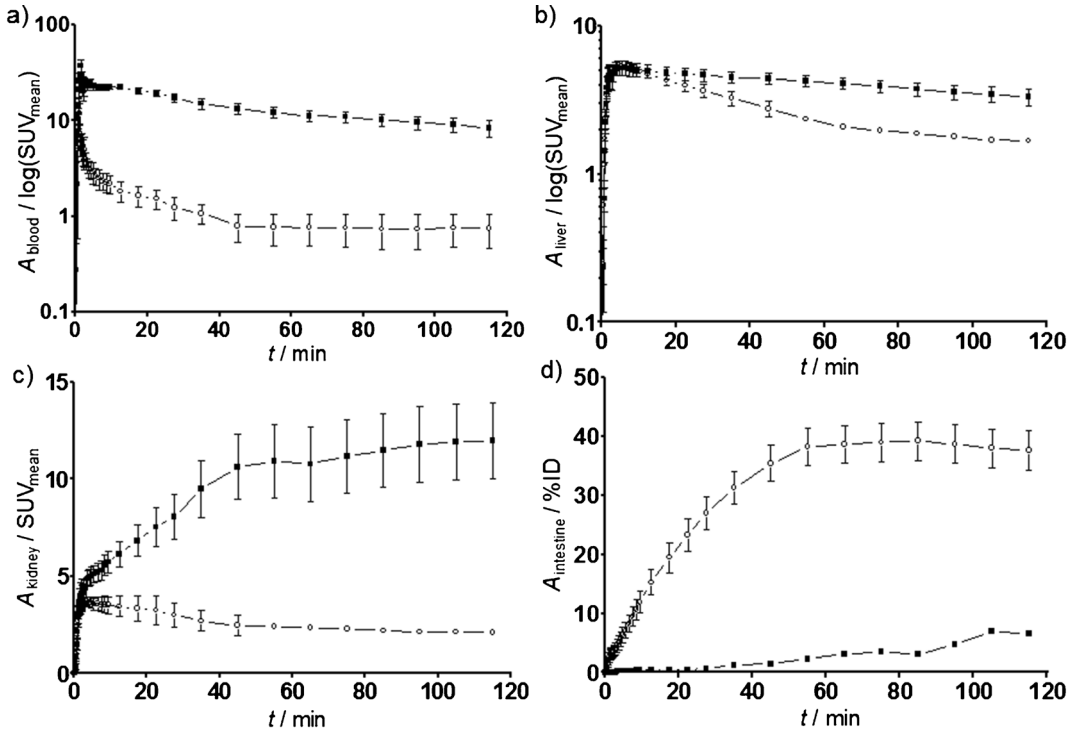

Figure 8. Biokinetics of [^{18}F]**3** in rats (■) and mice (○). The time–activity curves were derived from the regions of interest over a) the vena cava, b) the liver, c) the kidneys, and d) the intestine. Curves a)–c) are means ± SEM for five mice and eight rats. The time–activity curve of the rat intestine could be drawn only from one rat, because of the limited field of view; the elimination into the intestine of the rat is shown in table S5 in the Supporting Information.

the pharmacokinetics of [^{18}F]**3** was found to be complex; after an increase of the tumour uptake to an SUV of 0.86 (2.5 %ID g^{-1}), the uptake decreases over the time without reaching a steady state (Figure 9). This reversibility was also reflected in the kinetic PET analyses, in which the reversible two-tissue compartment model successfully described the tumour accumulation of [^{18}F]**3**. This model is defined by the following rate constants: K_1 (apparent influx rate constant), k_2 (efflux rate constant), k_3 (local uptake rate constant) and k_4 (rate constant of local release), the fractional blood volume (FBV), and the delay of tumour-tracer uptake in comparison with blood time activity in the vena cava and the aorta (see figure S9 in the Supporting Information for a schematic representation).[49] The ^{18}F-activity values were corrected for metabolites. The following values were calculated: $K_1 = 0.034$ min^{-1} mL^{-1}, $k_2 = 0.483$ min^{-1}, $k_3 = 0.082$ min^{-1}, $k_4 = 0.026$ min^{-1}, FBV = 0.012. The fractional blood volume (1.2 %) was relatively low; this seems to be a result of the artificially high interstitial pressure that is often observed in subcutaneously xenotransplanted tumours. The volume of distribution (V_T), which is equal to the ratio of tissue and plasma concentrations at true equilibrium, was 0.292 mL cm^{-3}. The low FBV might be caused by limited vascularisation. The tumour to muscle ratio increased up to 10 after two hours, which indicated specific interactions of [^{18}F]**3** in the tumour (Figure 9). As the presence of all four cathepsins that were investigated for inhibition by azadipeptide nitrile **3** could be confirmed immunohistochemically in the neoplastic tissue, a cathepsin-mediated tumour uptake of [^{18}F]**3** appears to be obvious. Injection of leupeptin (10 mg kg^{-1} body weight) 20 min before administration of [^{18}F]**3** did not block the tumour uptake of the radiotracer (see figure S10 in the Supporting Information). This does not necessarily indicate a cathepsin-independent mechanism for tumour accumulation. Similarly to azadipeptide nitrile **3**, the peptide aldehyde leupeptin interacts covalently with the active-site cysteine residue of cathepsins.[50] We assume that leupeptin, similarly to compound **3**, reacts spontaneously with other endogenous thiols and, therefore, protected [^{18}F]**3** from nonspecific interactions with thiols. In consequence, more unmetabolised [^{18}F]**3** should be available for tumour uptake. Such a phenomenon has also been observed with other radiotracers.[51]

Conclusions

The radiosynthesis of a fluorine-18-labelled PET tracer targeting cathepsins was established for the first time on the basis of compound **3**, a fluoroethylated inhibitor of the azadipeptide nitrile chemotype. Among different approaches tried, a two-step, one-pot procedure with 2-[^{18}F]fluoroethylnosylate was revealed to be the most efficient one for achieving sufficient and reproducible radiochemical yields in the radiosynthesis of [^{18}F]**3**.

The radiopharmacological characterisation of the tracer compound provided insight into the pharmacokinetic properties of azadipeptide nitriles. Their inherent thiol reactivity leads to a slow blood clearance, which limits their suitability as radiotracers for PET imaging.

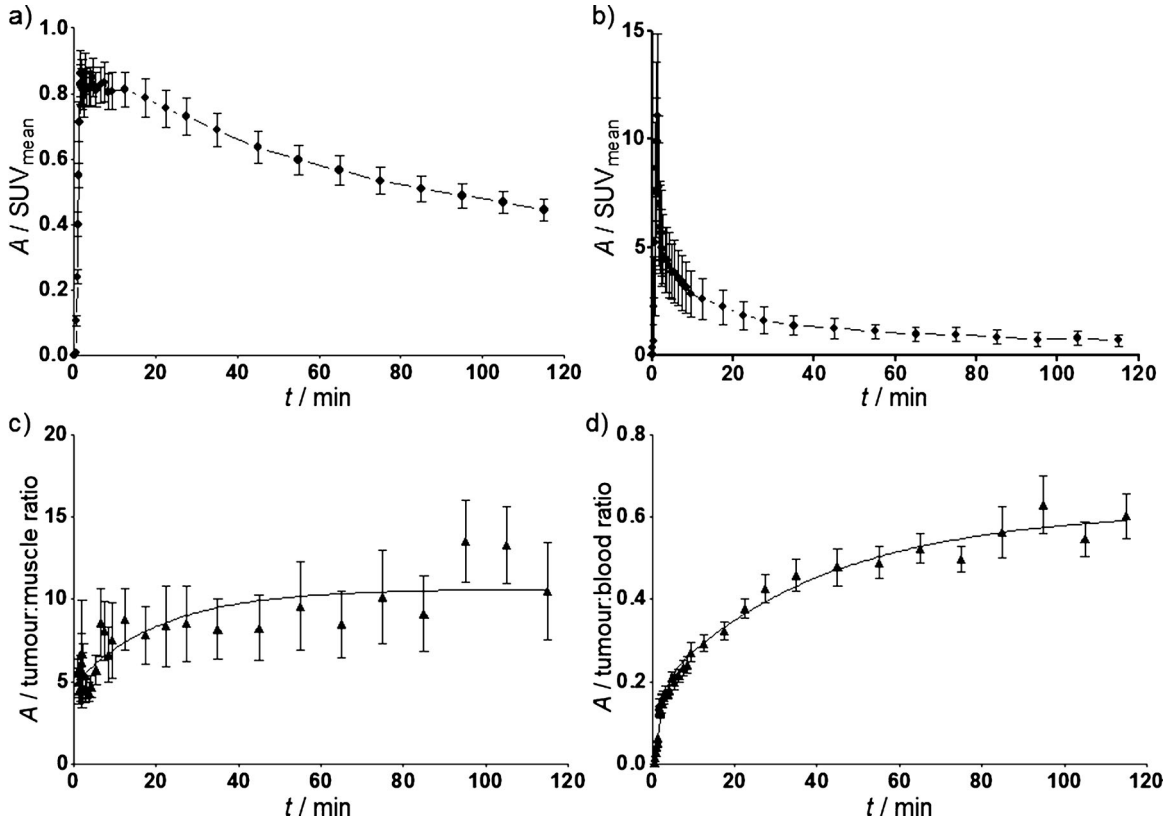

Figure 9. [^{18}F]**3** kinetics in NCI-H292 tumour-bearing mice. The time–activity curves represent a) tumour, b) blood, c) tumour-to-muscle and d) tumour-to-blood ratios. The values are means ± SEM for nine animals.

Dynamic PET studies with [^{18}F]**3** in NMRI nu/nu mice bearing tumours derived from the human lung carcinoma cell line NCI-H292 indicated a reversible tumour accumulation of the tracer. The kinetics of this process could be well described with a reversible two-tissue compartment model. Immunohistochemical analysis of the tumour sections for the presence cathepsins L, S, K and B confirmed the expression of the target enzymes. In combination, these results reveal strong evidence that [^{18}F]**3** is able to visualise tumour-associated cathepsins in vivo. The correlation of tumour uptake and tumour-associated cathepsin activity will be elaborated in further studies, together with the investigation of the radiotracer in other tumour models.

Experimental Section

Syntheses of reference compounds and precursors

General remarks: All commercial reagents and solvents were used without further purification unless otherwise specified. NMR spectra were recorded on a Varian Unity 400 MHz and on a Bruker Avance 500 MHz spectrometer. NMR chemical shifts were referenced with the residual solvent resonances relative to tetramethylsilane (TMS). The IR spectrum was recorded on a Bruker Tensor 27 FTIR spectrometer. Mass spectra were obtained on a Quattro/LC mass spectrometer (Micromass) by electrospray ionisation. LC-DAD chromatograms and ESI-MS spectra were recorded on an Agilent 1100 HPLC system with an Applied Biosystems API-2000 mass spectrometer. Preparative column chromatography was carried out by using Merck silica gel (mesh size 230–400 ASTM) with solvent mixtures as specified for the particular compounds. TLC was performed on Merck silica gel F-254 aluminium plates with visualisation under UV (254 nm). Radio-TLC was conducted in the same way with petroleum ether/EtOAc (1:2) as the eluent. Radioactive spots were visualised by using the Fujix Bas2000 TR radioluminography system. The identity of the radioactive spots was proven with the corresponding non-radioactive reference compounds that were spotted with radioactivity after visualisation under UV.

Analytical radio-HPLC was performed on a Luna C_{18} 5 μm column (Phenomenex, 250×4.6 mm) by using 50% CH_3CN/H_2O containing 0.1% trifluoroacetic acid as an isocratic eluent pumped by a Merck Hitachi L7100 gradient pump at a flow rate of 1 mL min^{-1} through a Jasco DG2080 4-line degasser with UV detection by a Merck Hitachi L7450 diode array detector and γ detection by a Raytest GABI detector. The system was operated by the D-700 HSM software with a Merck Hitachi D7000 interface. Semi-preparative radio-HPLC was done on a Nucleodur C_{18} Isis 5 μm column (Macherey–Nagel, 250×10 mm) by using 50% CH_3CN/H_2O containing 0.1% trifluoroacetic acid as an isocratic eluent (degassed before use by ultrasonication) pumped by a Jasco PU1580 pump at a flow rate of 4 mL min^{-1} with UV detection at 254 nm by a Jasco UV1575 detector. Sample injection was accomplished in an automated manner by using the equipment of a Nuclear Interface radiofluorination module that also contained the γ detector.

2-Bromo-1-fluoroethane (2): 2-Bromoethanol (1.8 mL, 25 mmol) was added to a solution of DAST (2.7 mL, 20 mmol) in diglyme (15 mL) at −50 °C. Cooling was continued for 30 min and the reaction mixture was stirred at room temperature for 14 h. The reaction

mixture was distilled at atmospheric pressure to obtain **2** (0.51 g, 16%) as a colourless liquid; ^{1}H NMR (400 MHz, $CDCl_3$): $\delta = 3.55$ (dt, $^3J_{H,F} = 20.1$ Hz, $^3J = 5.9$ Hz, 2H, CH_2Br), 4.67 ppm (dt, $^2J_{H,F} = 46.7$ Hz, $^3J = 5.9$ Hz, 2H, FCH_2); ^{19}F NMR (376 MHz, $CDCl_3$): $\delta = -212.4$ ppm (m).

***N*-(Benzyloxycarbonyl)-(*O*-(2-fluoroethyl)tyrosine)-methylazalanine-nitrile (3)**: Compound **1**[31a] (1.28 g, 3.35 mmol) was dissolved in dry DMF (20 mL) and cooled to −10 °C. The resulting solution was treated with NaH (0.14 g (60% in mineral oil), 3.50 mmol) and stirred at −10 °C for 30 min. Compound **2** (0.83 g (77% purity), 5.03 mmol) was added. The solution was slowly warmed to room temperature and stirred for 19 h. The solvent was removed under reduced pressure and the resulting residue was suspended in H_2O and extracted with EtOAc (3×30 mL). The combined organic layers were washed with H_2O (30 mL) and brine (30 mL), then dried over Na_2SO_4. The crude product was purified by column chromatography with EtOAc/petroleum ether (1:1) as the eluent to obtain **3** as colourless oil (0.53 g, 37%); $[\alpha]_D^{20} = +22.4$ ($c = 0.77$, $CHCl_3$); ^{1}H NMR (500 MHz, [D$_6$]DMSO, mixture of rotamers): $\delta = 2.73$–2.86 (m, 2H, CHC*H*$_2$), 2.98, 3.08, 3.12, 3.22 (4×s, 6H, 2×NCH$_3$), 4.19 (dt, $^3J_{H,F} = 30.0$ Hz, $^3J = 3.5$ Hz, 2H, OC*H*$_2$CH$_2$F), 4.66–4.77 (m, 3H, OCH$_2$C*H*$_2$F, NHC*H*CO), 4.95 (s, 2H, CH_2O), 6.88–7.34 (m, 9H, H_{arom}), 7.78$_a$, 7.87$_b$ ppm (br s$_a$, d$_b$, $^3J = 7.9$ Hz, 1H, N*H*CHCO); ^{13}C NMR (125 MHz, [D$_6$]DMSO, mixture of rotamers): $\delta = 30.28$, 30.59, 35.65, 36.04, 40.48, 40.88 (2×NCH$_3$, CHCH$_2$), 52.89, 53.34 (NHCHCO), 65.62 (CH_2O), 67.13 (d, $^2J_{C,F} = 18.8$ Hz, OCH$_2$CH$_2$F), 82.28 (d, $^1J_{C,F} = 165.6$ Hz, OCH$_2$CH$_2$F), 114.21, 114.57, 127.74, 127.91, 128.42, 129.85, 130.28, 130.50, 136.91 (CN, C_{arom}), 156.28 (OCON), 157.12 (C_{arom}O), 173.50 ppm (NHCH*C*O); FTIR (KBr): $\tilde{\nu} = 2222$ cm^{-1} (C≡N); LC-MS(ESI) (90% H_2O to 100% MeOH in 20 min, then 100% MeOH for 30 min; DAD: 219.7–300.7 nm): $t_R = 17.23$, 96% purity, $m/z = 429.5$ $[M+H]^+$.

Ethylene glycol dinosylate (5b): Nosyl chloride (10.64 g, 48 mmol) as a solid was added to a solution of ethylene glycol (1.12 mL, 20 mmol) in $CHCl_3$ (20 mL) and tetrahydrofuran (THF; 10 mL). Pyridine (6.46 mL, 80 mmol) was added dropwise to the resulting mixture under ice cooling. After the reaction mixture had stirred for 4 h at room temperature, the precipitate was collected by filtration and recrystallised from acetone (100 mL). The crystallised solid was collected by filtration, washed with a small amount of ice-cold acetone, petroleum ether and diethyl ether and recrystallised again from acetone to yield **5b** (3.38 g, 38%) as slightly yellow crystals; mp: 185 °C (lit.:[52] 186 °C); ^{1}H NMR (400 MHz, [D$_6$]DMSO): $\delta = 4.38$ (s, 4H, 2×CH$_2$), 8.13 (d, $^3J = 9.0$ Hz, 4H, 2′-H, 6′-H), 8.44 ppm (d, $^3J = 8.9$ Hz, 4H, 3′-H, 5′-H); ^{13}C NMR (101 MHz, [D$_6$]DMSO): $\delta = 69.6$ (CH_2), 125.6 (C-3′, C-5′), 130.1 (C-2′, C-6′), 140.7 (C-1′), 151.8 ppm (C-4′); elemental analysis: calcd for $C_{14}H_{12}N_2O_{10}S_2$: C 38.80, H 2.80, N 6.48, S 14.83; found: C 38.85, H 2.72, N 6.57, S 15.03.

3,4-Dibromobenzenesulfonyl chloride (4): Chlorosulfonic acid (8 mL, 120.1 mmol) was added dropwise to a solution of 1,2-dibromobenzene (1.8 mL, 15.1 mmol) in $CHCl_3$ (40 mL) at −10 °C. The reaction mixture was stirred for 24 h at room temperature and heated at reflux for 1 h, before being cooled and poured onto crushed ice (50 g). The organic layer was separated and the aqueous phase was extracted with CH_2Cl_2. The combined organic layers were washed with sat. $NaHCO_3$, H_2O (2×20 mL) and brine (20 mL) and dried over Na_2SO_4. The solvent was removed in vacuo and the remaining residue was purified by vacuum distillation (0.038 mbar, 120 °C) to obtain **4** (2.96 g, 77%) as a yellowish waxy solid; mp: 38–40 °C (lit.:[53] 34 °C); ^{1}H NMR (400 MHz, $CDCl_3$): $\delta = 7.82$ (dd, $^3J = 8.5$ Hz, $^4J = 2.3$ Hz, 1H, H-6), 7.89 (d, $^3J = 8.5$ Hz, 1H, H-5), 8.26 ppm (d, $^4J = 2.2$ Hz, 1H, H-2).

Ethylene glycol-1,2-bis(3,4-dibromobenzenesulfonate) (5c): Potassium trimethylsilanolate (1.92 g, 14.96 mmol) was added as a solid in portions to a solution of ethylene glycol (0.19 g, 2.99 mmol) and **4** (2.5 g, 7.48 mmol) in THF (6 mL) under ice cooling. The reaction mixture was stirred for 2 h in the ice bath and subsequently diluted with ice-cold H_2O (30 mL) and CH_2Cl_2 (20 mL). The aqueous layer was extracted with CH_2Cl_2 (2×20 mL) and the combined organic phases were washed with brine (20 mL), dried over Na_2SO_4 and evaporated in vacuo. The obtained crude product was recrystallised from petroleum ether/$CHCl_3$ to yield **5c** (0.51 g, 26%) as white needles; mp: 167–168 °C (lit.:[35] 168 °C); ^{1}H NMR (400 MHz, $CDCl_3$): $\delta = 4.31$ (s, 4H, 2×CH$_2$), 7.64 (dd, $^3J = 8.4$ Hz, $^4J = 2.2$ Hz, 2H, H-6, H-6′), 7.83 (d, $^3J = 8.4$ Hz, 2H, H-5, H-5′), 8.09 ppm (d, $^4J = 2.2$ Hz, 2H, H-2, H-2′); MS (ESI, positive): $m/z = 681$ $[M+Na]^+$; elemental analysis: calcd for $C_8H_{10}Br_4O_6S_2$: C 25.56, H 1.53, S 9.75; found: C 25.61, H 1.42, S 9.90.

2-Fluoroethyltosylate (6a): Tosyl chloride (2.23 g, 11.7 mmol), triethylamine (1.62 mL, 11.7 mmol) and 4-dimethylaminopyridine (0.11 g, 0.12 mmol) were successively added to a solution of 2-fluoroethanol (0.45 mL, 7.8 mmol) in dry CH_2Cl_2 (17 mL) under ice cooling. After it had been stirred for 2 h at room temperature, the reaction mixture was diluted with CH_2Cl_2 (20 mL) and 1 M HCl (20 mL) was added. The organic layer was separated and the aqueous phase was extracted with CH_2Cl_2 (2×20 mL). The combined organic layers were washed with sat. $NaHCO_3$ and brine (20 mL each), dried over Na_2SO_4 and evaporated to dryness. The obtained residue was purified by column chromatography on silica gel (petroleum ether/EtOAc, 4:1) to yield **6a** (1.12 g, 66%) as a yellowish oil; ^{1}H NMR (400 MHz, $CDCl_3$): $\delta = 2.46$ (s, 3H, CH_3), 4.20 (dt, $^3J_{H,F} = 27.0$ Hz, $^3J = 4.2$ Hz, 2H, CH_2O), 4.50 (dt, $^2J_{H,F} = 47.0$ Hz, $^3J = 4.1$ Hz, 2H, FCH_2), 7.36 (d, $^3J = 8.0$ Hz, 2H, H-3′, H-5′), 7.81 ppm (d, $^3J = 8.4$ Hz, 2H, H-2′, H-6′); MS (ESI, positive): $m/z = 241$ $[M+Na]^+$; elemental analysis: calcd for $C_9H_{11}FO_3S$: C 49.53, H 5.00, S 14.69; found: C 49.39, H 5.11, S 14.63.

2-Fluoroethylnosylate (6b): A solution of nosyl chloride (0.42 g, 1.9 mmol) in THF (3 mL) and potassium trimethylsilanolate (0.87 g, 6.8 mmol) as a solid were added to a solution of 2-fluoroethanol (0.078 mL, 1.36 mmol) in THF (2 mL) under ice cooling. The resulting brownish slurry was stirred for 2 h at 4 °C. H_2O (30 mL) was added and the mixture extracted with CH_2Cl_2 (3×20 mL). The combined organic layers were washed with brine (20 mL), dried over Na_2SO_4 and evaporated to dryness. The obtained residue was purified by column chromatography on silica gel (petroleum ether/EtOAc, 4:1) to yield **6b** (0.20 g, 59%) as an off-white solid; mp: 116–119 °C (lit.:[35] 118 °C); ^{1}H NMR (400 MHz, $CDCl_3$): $\delta = 4.41$ (dt, $^3J_{H,F} = 27.3$ Hz, $^3J = 4.20$ Hz, 2H, CH_2O), 4.60 (dt, $^2J_{H,F} = 47.0$ Hz, $^3J = 4.1$ Hz, 2H, FCH_2), 8.14 (d, $^3J = 9.0$ Hz, 2H, H-2′, H-6′), 8.42 ppm (d, $^3J = 9.0$ Hz, 2H, H-3′, H-5′); MS (ESI, positive): $m/z = 457$ $[M+5CH_3CN+H]^+$.

2-Fluoroethyl-3,4-dibromobenzenesulfonate (6c): Potassium trimethylsilanolate (0.87 g, 6.8 mmol) was added as a solid in portions to a solution of 2-fluoroethanol (0.08 mL, 1.4 mmol) and **4** (0.57 g, 1.7 mmol) in THF (2 mL) under ice cooling. The reaction mixture was stirred for 2 h in the ice bath and subsequently diluted with ice-cold H_2O (30 mL) and CH_2Cl_2 (20 mL). The aqueous layer was extracted with CH_2Cl_2 (2×20 mL) and the combined organic phases were washed with sat. $NaHCO_3$ (20 mL) and brine (20 mL), dried over Na_2SO_4 and evaporated in vacuo to yield **6c** (0.28 g, 57%) as a yellow solid; mp: 67–69 °C (lit.:[35] 68–70 °C); ^{1}H NMR (400 MHz, $CDCl_3$): $\delta = 4.35$ (dt, $^3J_{H,F} = 27.1$ Hz, $^3J = 4.0$ Hz, 2H, H-7a, H-7b), 4.61 (dt, $^2J_{H,F} = 47.1$ Hz, $^3J = 4.1$ Hz, 2H, H-8a, H-8b), 7.70 (dd, $^3J = 8.4$ Hz, $^4J = 2.2$ Hz, 1H, H-6), 7.83 (d, $^3J = 8.4$ Hz, 1H, H-

5), 8.16 ppm (d, ^4J = 2.1 Hz, 1H, H-2); ^{13}C NMR (101 MHz, $CDCl_3$): δ = 69.25 (C-7), 81.38 (C-8), 126.26, 127.53, 132.15, 132.96, 134.75, 136.26 ppm (C_{arom}); elemental analysis: calcd for $C_8H_7Br_2FO_3S$: C 26.54, H 1.95, S 8.86; found: C 27.13, H 1.91, S 8.98.

(*S*)-2-(4-(2-(Benzyloxycarbonylamino)-3-(2-cyano-1,2-dimethylhydrazinyl)-3-oxopropyl)phenoxy)ethyl-4-methylbenzenesulfonate (7a): Ethylene glycol-1,2-ditosylate (**5a**; 0.35 g, 0.94 mmol) and potassium carbonate (0.04 mg, 0.3 mmol) were added as solids to a solution of **1** (0.2 g, 0.52 mmol) in CH_3CN (6 mL). The resulting mixture was heated at reflux for 6 h. After cooling, the reaction mixture was acidified with 1 M HCl (20 mL) and extracted with EtOAc (3×30 mL). The combined organic layers were washed with brine and dried over Na_2SO_4. The crude product obtained after evaporation of the solvent was purified by column chromatography (CH_2Cl_2/MeOH, 150:1) to yield **7a** (0.11 g, 37%) as a colourless waxy solid; mp: 40–44 °C; ^{1}H NMR (400 MHz, $CDCl_3$, mixture of rotamers, only the signals of the major rotamer are listed): δ = 2.45 (s, 3H, Ts-CH_3), 2.83 (dd, ^2J = 14.1 Hz, ^3J = 8.1 Hz, 1H, $C_\beta H$H), 3.05 (dd, ^2J = 14.0 Hz, ^3J = 5.5 Hz, 1H, C_βH*H*), 3.20 (s, 3H, NCH_3), 3.24 (s, 3H, NCH_3), 4.09–4.14 (m, 2H, CH_2OTs), 4.31–4.38 (m, 2H, PhOCH_2), 4.95–5.18 (m, 3H, PhCH_2O, C_αH), 5.26 (d, ^3J = 8.4 Hz, 1H, NH), 6.72 (d, ^3J = 8.4 Hz, 2H, PhO-*o*H), 7.06 (d, ^3J = 8.4 Hz, 2H, PhO-*m*H), 7.26–7.40 (m, 7H, Ph, Ts-H-3′, Ts-H-5′), 7.82 ppm (d, ^3J = 8.3 Hz, 2H, Ts-H-2′, Ts-H-6′); ^{13}C NMR (101 MHz, $CDCl_3$): δ = 21.81 (C-24), 30.61, 37.78, 41.43 (C-10, C-11, C-13), 52.17 (C-8), 65.62, 67.33, 68.23 (C-5, C-18, C-19), 113.56 (C-12), 115.10 (C-16, C-16′), 128.18, 128.39, 128.68, 129.99, 130.10, 130.44, 130.76, 136.11, 145.06, 145.41 (C_{arom}), 156.07, 157.49 (C-17, C-6), 173.40 ppm (C-9); elemental analysis: calcd for $C_{29}H_{32}N_4O_7S$: C 59.99, H 5.55, N 9.65, S 5.54; found: C 59.38, H 5.55, N 9.19, S 5.59.

(*S*)-2-(4-(2-(Benzyloxycarbonylamino)-3-(2-cyano-1,2-dimethylhydrazinyl)-3-oxopropyl)phenoxy)ethyl-4-nitrobenzenesulfonate (7b): The procedure described for the synthesis of **7a** was followed, with the exception that **5b** (0.40 g, 0.94 mmol) was used instead of **5a** and the reaction time was decreased to 2 h. Compound **7b** (0.10 g, 31%) was obtained as a yellow solid; mp: 74–79 °C; ^{1}H NMR (400 MHz, $CDCl_3$, mixture of rotamers, only the signals of the major rotamer are listed): δ = 2.84 (dd, ^2J = 14.0 Hz, ^3J = 7.7 Hz, 1H, $C_\beta H$H), 3.03 (dd, ^2J = 14.0 Hz, ^3J = 5.7 Hz, 1H, C_βH*H*), 3.19 (s, 3H, NCH_3), 3.23 (s, 3H, NCH_3), 4.12–4.18 (m, 2H, CH_2ONs), 4.46–4.52 (m, 2H, PhOCH_2), 4.96–5.18 (m, 3H, PhCH_2O, C_αH), 5.27 (d, ^3J = 8.8 Hz, 1H, NH), 6.65 (d, ^3J = 8.5 Hz, 2H, PhO-*o*H), 7.05 (d, ^3J = 8.5 Hz, 2H, PhO-*m*H), 7.38–7.27 (m, 5H, Ph), 8.11 (d, ^3J = 8.8 Hz, 2H, Ns-H-2′, Ns-H-6′), 8.35 ppm (d, ^3J = 8.5 Hz, 2H, Ns-H-3′, Ns-H-5′); ^{13}C NMR (101 MHz, $CDCl_3$): δ = 30.57, 37.83, 41.42 (C-10, C-11, C-13), 52.10 (C-8), 65.40, 67.23, 69.60 (C-5, C-18, C-19), 113.51 (C-12), 114.98 (C-16, C-16′), 124.55, 128.16, 128.41, 128.62, 128.69, 129.42, 130.52, 130.82 (C_{arom}), 141.95, 150.91, 156.06, 157.12 (C-20, C-23, C-17, C-6), 173.35 ppm (C-9); elemental analysis: calcd for $C_{28}H_{29}N_5O_9S$: C 54.98, H 4.78, N 11.45, S 5.24; found: C 53.06, H 5.04, N 10.77, S 4.85.

Radiosynthesis

Processing of [^{18}F]fluoride for radiosynthesis: No-carrier-added aqueous [^{18}F]HF was produced in a IBA CYCLONE 18/9 cyclotron by irradiation of [^{18}O]H_2O through the ^{18}O(p,n)^{18}F nuclear reaction. The aqueous [^{18}F]fluoride (500–3000 MBq) was adsorbed on an anion-exchange cartridge (QMA plus, Waters) and eluted with a solution (1 mL) of 26.6 mM Kryptofix 222 and 13.4 mM K_2CO_3 in 14% H_2O/CH_3CN into a conical glass vial equipped with a screw cap and rubber septum. Removal of H_2O was accomplished by azeotropic distillation with CH_3CN in a stream of nitrogen gas at 90 °C with stirring. In total, 4×2 mL of CH_3CN were added and the remaining residue was dissolved in the corresponding reaction medium.

Preparation of 2-[^{18}F]fluoroethylbenzenesulfonates: A solution of the appropriate ethylene dibenzenesulfonate (**5a–c**) in CH_3CN (1 mL) was added to the [^{18}F]KF-containing residue obtained by azeotropic distillation and brought to the reaction temperature of 90 °C in the screw-cap-sealed vial. To optimise the reaction with regard to the amount of precursor and time, 10 μL aliquots of the reaction were withdrawn after 5, 10 and 15 min, diluted with CH_3CN (90 μL) and analysed by radio-TLC.

Conditions for ^{18}F-fluoroethylations: A solution of **1** (1.5-fold excess related to the corresponding ethylene dibenzenesulfonate) in CH_3CN (or DMF; 100 μL) was added to the solution containing the 2-[^{18}F]fluoroethylbenzenesulfonate, followed by a 1 M solution of Cs_2CO_3 in H_2O (volume corresponding to an amount equimolar to **1**). The conditions were specified in the Results and Discussion section. When the ^{18}F-fluoroethylation was performed in DMF, the solution of [^{18}F]**6a** in CH_3CN obtained after reaction with [^{18}F]fluoride was evaporated in the nitrogen stream and the obtained residue was redissolved in DMF (1 mL).

Conversion of the direct precursors 7a and 7b with [^{18}F]fluoride: A solution containing **7a** or **7b** (1, 3 or 5 mg) in CH_3CN (1 mL) was added to the [^{18}F]KF-containing residue obtained by azeotropic distillation and brought to the reaction temperature of 90 °C. Aliquots (10 μL) were withdrawn after 5, 10 and 15 min, diluted with CH_3CN (90 μL each) and analysed by radio-TLC.

Preparation of [^{18}F]3 by the optimised procedure: A solution of **5b** (5 mg, 11.6 mmol) in CH_3CN (1 mL) was added to the [^{18}F]KF-containing residue obtained by azeotropic distillation and brought to the reaction temperature of 90 °C for 5 min. The reaction solution was cooled to 4 °C. A solution of **1** (6.65 mg, 15.5 mmol) in CH_3CN (100 μL) was added, followed by 1 M Cs_2CO_3 in H_2O (15.5 μL). The resulting mixture was heated at 115 °C for 10 min and subsequently cooled to 4 °C. The solution was diluted with 0.1% CF_3COOH/H_2O (1 mL) and filtered. The filtrate was transferred into a hot cell and purified by semi-preparative radio-HPLC. The peak representing the product was collected and immediately diluted with H_2O (30 mL). The resulting solution was subjected to solid-phase extraction by using a 500 mg LiChrolut RP-18E (40–63 μm) cartridge. The cartridge was washed with H_2O (3 mL) and the product was eluted with 2×0.5 mL of EtOH. The product solution was completely evaporated and the obtained residue was redissolved in EtOH (55 μL). A 5 μL aliquot of the final product solution was withdrawn, diluted with CH_3CN (50 μL) and used for quality control by radio-HPLC and radio-TLC.

Enzyme inhibition assays

Cathepsin assays were performed as described previously.[31a]

Immunohistochemistry of tumour and organ sections

Tumour and organ pieces were fixed in 4% phosphate-buffered paraformaldehyde, paraffin-embedded, cut into 5 μm sections and mounted onto SuperFrostPlus object slides. Tissue sections were rehydrated and pretreated in 500 mM tris(hydroxymethyl)aminomethane (Tris)/10 mM ethylenediaminetetraacetate (EDTA; pH 9.0) or 10 mM citrate buffer (pH 6.0, staining of cathepsin S) heated for 20 min by microwave. After blocking unspecific binding sites with

a solution containing 0.3% milk powder, 0.1% gelatin and 2% bovine serum albumin in Tris-buffered saline containing 0.05% Tween 20 (TBS-0.05% Tween 20; pH 7.4), the primary antibody was incubated at 4 °C overnight. Cathepsins were visualised by using antibodies from Abcam (cathepsin L: mouse monoclonal #ab6314, dilution 1:100; cathepsin S: goat polyclonal #ab18822, dilution 1:40; cathepsin B: rabbit polyclonal #ab33538, dilution 1:200; cathepsin K: rabbit polyclonal #ab19027, dilution 1:100; typical volumes were 50–100 μL each). After washing with TBS-0.05% Tween 20 (pH 7.4; 3×10 min), primary antibodies were visualised with the corresponding biotinylated secondary antibodies goat anti-rabbit, goat anti-mouse or donkey anti-goat (Dianova, dilution 1:200, 1–2 h incubation time), followed by incubation with ExtrAvidin peroxidase (Sigma–Aldrich) and the AEC substrate kit (BD Pharmingen). Finally, tumour sections were counterstained by using Mayer's Hematoxylin and embedded in glycerol. Slides were analysed by using an AxioImager.A1 microscope and the appropriate AxioVision software package (Carl Zeiss MicroImaging).

Chemical stability, distribution coefficient, in vitro stability, and cell uptake experiments

Chemical stability: [^{18}F]**3** (10–20 MBq) dissolved in EtOH was diluted 1:10 or 1:20 in different buffered aqueous media and incubated at 37 °C in a thermomixer. Aliquots of 20 μL were withdrawn after 0, 1, 2, 3, 4 and 5 h, diluted with CH_3CN (100 μL) and spotted on a TLC plate (10 μL). In addition, non-radioactive **3** was spotted. The TLC plate was developed in petroleum ether/EtOAc (2:1) and visualised under UV as well as by radioluminography, as described above. The aqueous media used were 0.1 M sodium phosphate (pH 6.0), 10×PBS (pH 7.4), and 10×TBS (pH 8.0).

Water–octanol distribution coefficient: [^{18}F]**3** (~5 MBq) dissolved in 10% EtOH/H_2O (100 μL) was added to a mixture of *n*-octanol (5 mL) and H_2O (5 mL) in a shaking flask. After vigorous shaking, the separated aqueous phase was discarded and H_2O (5 mL) was added to the shaking flask. After shaking again, 3×100 μL of each layer were transferred to scintillation vials, each containing H_2O (1 mL), and the activities (*A*) were measured in a γ counter. The values were averaged and the log*P* value was calculated according to $\log P = \log(A(\text{organic phase})/A(\text{aqueous phase}))$.

In vitro and in vivo stability: In order to investigate in vitro stability, [^{18}F]**3** was incubated at 37 °C with venous blood obtained from male Wistar rats. The time points of analysis corresponded to those used in the studies of in vivo stability. The latter were carried out on arterial blood samples that were collected from the right femoral artery at 1, 3, 5, 10, 20, 30 and 60 min after intravenous administration of [^{18}F]**3**.

Blood cells were separated by centrifugation (5 °C, 5 min, 8000 rpm) and plasma proteins were precipitated by using 60% acetonitrile and subsequent centrifugation (5 °C, 5 min, 8000 rpm). The supernatant was analysed by radio-HPLC. The radio-HPLC system (Agilent 1100 series) applied for metabolite analysis was equipped with UV detection (254 nm) and an external radiochemical detector (RAMONA, Raytest GmbH, Straubenhardt, Germany). Analysis was performed on a Zorbax C_{18} 300SB (250×9.4 mm; 4 μm) column with an eluent system comprising C (H_2O with 0.1% trifluoroacetic acid (TFA)) and D (acetonitrile with 0.1% TFA) with a gradient of 5 min 95% C, 10 min to 95% D and 5 min at 95% D at a flow rate of 3 mL min^{-1}. HPLC were performed on [^{18}F]**3** added to a rat blood sample, on arterial blood samples from 1 to 60 min after injections and on a urine sample from 60 min after injection. The metabolite fraction in the blood was calculated as a percentage of the parent compound in the blood from the HPLC. The extracts from other tissues, urine or intestine content were prepared by ultrasound homogenisation as a 10% solution in PBS, centrifugation (5 °C, 70000 g×min) and subsequent precipitation by 60% acetonitrile. The supernatant was analysed by the described radio-HPLC.

Experiments to suppress conjugate formation between [^{18}F]**3** and glutathione were performed with whole rat blood as noted above. Solutions of 10 mM buthionine sulfoximine (BSO; purchased from Sigma, diastereomeric mixture with varying chirality at the sulfur atom) in PBS and 50 mM etacrynic acid in EtOH were freshly prepared. Blood samples (each 400 μL) were treated with BSO (80, 160 or 240 μL) and incubated for 2 h (final concentrations of BSO: 1.67, 2.56 and 3.75 mM, respectively). [^{18}F]**3** was added and the samples were analysed by radio-HPLC as described above. In a further experiment, etacrynic acid (40 μL) was added to each of the blood samples in addition to BSO (final concentrations of etacrynic acid: 3.85, 3.33 and 2.94 mM, respectively). Independently, blood samples were treated with diethylmaleate (DEM) in amounts that were 2% of the sample volume and incubated for 1 h before addition of [^{18}F]**3**.

In vivo experiments

Animal experiments were carried out according to the guidelines of the German Regulations for Animal Welfare. The protocol was approved by the local Ethical Committee for Animal Experiments.

Besides the in vivo stability studies, biodistribution and small-animal PET experiments were also performed in male Wistar rats.

For the in vivo stability studies, rats (aged 7–9 weeks, (183±56) g (mean body weight ± standard deviation (SD)), $n=19$) were anaesthetised with desflurane (initially 9%, then 6% in 20% oxygen/air). The guide value for breathing frequency was 65 breaths min^{-1}. Animals were put in the supine position and placed on a heating pad to maintain body temperature. The spontaneously breathing rats were treated with 100 units kg^{-1} heparin (Heparin-Natrium 25000-ratiopharm, Ratiopharm, Germany) by subcutaneous injection to prevent blood clotting on intravascular catheters. After local anaesthesia by injection of 1% Lignocaine (Xylocitin loc, Mibe, Jena, Germany) into the right groin, a catheter was introduced into the right femoral artery (0.8 mm Umbilical Vessel Catheter, Tyco Healthcare, Tullamore, Ireland) for blood samples for metabolite analysis, for gas analysis and for arterial blood pressure measurements; a second needle (35 G) catheter in one tail vein was used for administration of the [^{18}F]**3**.

From rat heparin blood, erythrocyte ghosts were also prepared. Heparin blood was centrifuged for 5000 g×min at 4 °C and the plasma and white cells were discarded. Packed erythrocytes were washed three times with isotonic chloride solution and, each time, the buffy coat was carefully removed. Red blood cells (1 mL) were added to deionised water (3 mL) at 4 °C and gently vortexed. At the end of the hypotonic hemolysis, the isotonicity was restored with isotonic sodium chloride (0.5 mL) and the erythrocytes were thus allowed to restore during 30 min. The restored cells were then washed three times with PBS and used within 4 h.

For biodistribution experiments, two groups of four rats (aged 7 to 9 weeks; mean body weight ± SD: (186±11) g) for each time point were intravenously injected into a tail vein with [^{18}F]**3** (~0.3 MBq) dissolved in E-153 electrolyte solution (0.5 mL). The specific activity ranged between 5 and 30 GBq mmol^{-1} at the time of injection. Animals were sacrificed at 5 and 60 min post injection. Blood and the

major organs were collected, weighed and counted in a Wallac WIZARD automatic γ counter (Perkin–Elmer, Germany). The radioactivity of the tissue samples was decay corrected and calibrated by comparing the counts in tissue with the counts in aliquots of the injected tracer that had been measured in the γ counter at the same time. The activity amount in the selected tissues and organs was expressed as percent injected dose (%ID). The activity concentration in the biodistribution measurements was calculated as SUV_{bio} (g/g, SUV = (activity per g of tissue)/(injected activity/body weight)) and expressed as the mean ± SD for each group of sixteen animals.

Additionally, small-animal PET experiments were performed in normal NMRI mice and NCI-H292 xenotransplanted NMRI nu/nu mice. With this aim, female NMRI (nu/nu) mice (10–14 weeks old) were purchased from the specific pathogen-free breeding facility of the Experimental Centre of the Medical Faculty Carl Gustav Carus, University of Technology, Dresden. For the generation of subcutaneous tumours, NCI-H292 cells (ATCC CRL-1848) were used. Tumour cells were harvested, washed in PBS and transferred to 0.9% sodium chloride. Only single-cell suspensions (5×10^6 cells per 100 μL) with at least 90% viability (trypan blue exclusion) were used for injection. Animals were anaesthetised by using desflurane (10% v/v in 30% oxygen/air) and tumour cells were subcutaneously injected into the right hind leg. Tumour size was monitored three times a week by calliper measurements and the tumour volume was calculated by using the formula $V=\pi/6\times$(tumour length × tumour width × tumour width). Animals entered the imaging study 15–20 days after tumour-cell injection with tumour volumes of 100–400 mm^3.

For small-animal PET experiments, anaesthetised, spontaneously breathing animals were allowed to stabilise for 10 min after preparation. A 10 min transmission scan was recorded during this time for each subject by using a rotating point source of ^{57}Co (microPET P4; Siemens preclinical solutions, Knoxville, TN) or a whole-body CT was recorded (NanoScan PET/CT; Mediso Budapest, Hungary). The transmission scans were used to correct the emission scan for γ-ray attenuation caused by body tissues and supporting structures; they were also used to demarcate the body field for image registration. The activity of the injection solution was measured in a well counter (Isomed 2000, Dresden, Germany) cross-calibrated to the small-animal PET scanners. The PET acquisition of 60- or 120 min emission scans was started and the infusion of the [^{18}F]**3** into a tail vein was initiated with a delay of 30 s. At the end of the experiment, the animals were deeply anaesthetised and sacrificed by an intravenous injection of potassium chloride.

Data acquisition was performed in 3D list mode. Emission data were collected continuously. The list mode data were sorted with 32 or 38 frames (15×10 s, 5×30 s, 5×60 s, 4×300 s, 3×600 s or 9×600 s). The data were decay, scatter and attenuation corrected. The frames were reconstructed by Ordered Subset Expectation Maximisation applied to 3D sinograms (OSEM3D). The voxel size was 0.06×0.06×0.12 cm and the resolution in the centre of the field of view was equal to or lower than 1.8 mm. The image volume data were converted into the Siemens ECAT7 format for further processing. The image files were then processed by using the ROVER software (ABX GmbH, Radeberg, Germany). Masks for defining three-dimensional regions of interest (ROIs) were set and the ROIs were defined by thresholding; ROI time–activity curves (TAC) were derived for the subsequent data analysis. The input curves were calculated from the ROIs over the vena cava by using a recovery of 26% and the ROIs over the tumours. No especially partial volume correction was applied because the background activity only minimally changed over the time of measurement. The ROI data and TAC were further analysed by using R (R is available as Free Software under the terms of the Free Software Foundation's GNU General Public License in source code form) and especially developed program packages (Jörg van den Hoff, Helmholtz-Zentrum Dresden-Rossendorf, Dresden, Germany). The standardised uptake values (SUV = (activity per mL of tissue)/(injected activity/body weight), g mL^{-1})) were calculated in the ROIs.

The standard reversible two-tissue compartment model[49] was fitted to the mean tumour time–activity curve of nine animals, with the mean blood time–activity derived input curve of nine animals. In the parameter estimation, the fractional blood volume and tracer delay at the tumour were included. The fitting was performed by the nonlinear "compfit" algorithm implemented in R by J. van den Hoff.

Statistical analyses

Data are expressed as mean ± SD. Values were compared by using an unpaired Student's t-test with Welch's correction and an F-test to compare the variances (GraphPad Prism 5.02 for Windows, GraphPad Software, San Diego, CA). The non-parametric Wilcoxon signed rank test and the D'Agostino–Pearson normality test were used for statistical evaluation for some of the data. A P value of <0.05 was considered significant and is indicated by an asterisk.

Acknowledgements

The dedicated assistance of Andrea Suhr, Natalie Thieme, and Regina Herrlich in the animal experiments is gratefully acknowledged. We cordially appreciate the expert support of Catharina Heinig, Aline Morgenegg, and Mareike Barth in the immunohistochemical analyses, as well as that of Stephan Preusche and his team for providing [^{18}F]fluoride. Further thanks are due to Dr. Torsten Knieß for radiochemical advice. This work is part of a research initiative within the Helmholtz-Portfoliothema "Technologie und Medizin—Multimodale Bildgebung zur Aufklärung des In-vivo-Verhaltens von polymeren Biomaterialien".

Keywords: cathepsins · fluorine · glutathione · imaging agents · positron emission tomography · radiochemistry

[1] a) J. M. Rothberg, M. Sameni, K. Moin, B. F. Sloane, *Biochim. Biophys. Acta Proteins Proteomics* **2012**, *1824*, 123–132; b) S. D. Mason, J. A. Joyce, *Trends Cell Biol.* **2011**, *21*, 228–237.
[2] E. I. Deryugina, J. P. Quigley, *Cancer Metastasis Rev.* **2006**, *25*, 9–34.
[3] F. Lecaille, J. Kaleta, D. Brömme, *Chem. Rev.* **2002**, *102*, 4459–4488.
[4] J. A. Joyce, A. Baruch, K. Chehade, N. Meyer-Morse, E. Giraudo, F. Y. Tsai, D. C. Greenbaum, J. H. Hager, M. Bogyo, D. Hanahan, *Cancer Cell* **2004**, *5*, 443–453.
[5] a) T. Nomura, N. Katunuma, *J. Med. Invest.* **2005**, *52*, 1–9; b) M. M. Mohamed, B. F. Sloane, *Nat. Rev. Cancer* **2006**, *6*, 764–775; c) T. Reinheckel, C. Peters, A. Krüger, B. Turk, O. Vasiljeva, *Front. Pharmacol.* **2012**, *3*, 133.
[6] V. Gocheva, J. A. Joyce, *Cell Cycle* **2007**, *6*, 60–64.
[7] a) J. Kos, T. T. Lah, *Oncol. Rep.* **1998**, *5*, 1349–1361; b) J. Kos, B. Werle, T. Lah, N. Brunner, *Int. J. Biol. Markers* **2000**, *15*, 84–89; c) I. Berdowska, *Clin. Chim. Acta* **2004**, *342*, 41–69.
[8] a) E. Fröhlich, B. Schlagenhauff, M. Möhrle, E. Weber, C. Klessen, G. Rassner, *Cancer* **2001**, *91*, 972–982; b) P. Matarrese, B. Ascione, L. Ciarlo, R. Vona, C. Leonetti, M. Scarsella, A. M. Mileo, C. Catricala, M. G. Paggi, W. Malorni, *Mol. Cancer* **2010**, *9*, 207.

[9] a) B. Gole, M. B. D. Alonso, V. Dolenc, T. Lah, *Pathol. Oncol. Res.* **2009**, *15*, 711 – 723; b) C. Colin, B. Voutsinos-Porche, I. Nanni, F. Fina, P. Metellus, D. Intagliata, N. Baeza, C. Bouvier, C. Delfino, A. Loundou, O. Chinot, T. Lah, J. Kos, P. M. Martin, L. Ouafik, D. Figarella-Branger, *Acta Neuropathol.* **2009**, *118*, 745 – 754.

[10] a) B. F. Sloane, S. Q. Yan, I. Podgorski, B. E. Linebaugh, M. L. Cher, J. X. Mai, D. Cavallo-Medved, M. Sameni, J. Dosescu, K. Moin, *Semin. Cancer Biol.* **2005**, *15*, 149 – 157; b) C. J. Watson, P. A. Kreuzaler, *J. Mammary Gland Biol. Neoplasia* **2009**, *14*, 171 – 179; c) L. Sevenich, U. Schurigt, K. Sachse, M. Gajda, F. Werner, S. Müller, O. Vasiljeva, A. Schwinde, N. Klemm, J. Deussing, C. Peters, T. Reinheckel, *Proc. Natl. Acad. Sci. USA* **2010**, *107*, 2497 – 2502; d) L. Sevenich, F. Werner, M. Gajda, U. Schurigt, C. Sieber, S. Müller, M. Follo, C. Peters, T. Reinheckel, *Oncogene* **2011**, *30*, 54 – 64; e) N. P. Withana, G. Blum, M. Sameni, C. Slaney, A. Anbalagan, M. B. Olive, B. N. Bidwell, L. Edgington, L. Wang, K. Moin, B. F. Sloane, R. L. Anderson, M. S. Bogyo, B. S. Parker, *Cancer Res.* **2012**, *72*, 1199 – 1209.

[11] K. Ravanko, K. Järvinen, J. Helin, N. Kalkkinen, E. Hölttä, *Cancer Res.* **2004**, *64*, 8831 – 8838.

[12] N. Rousselet, L. Mills, D. Jean, C. Tellez, M. Bar-Eli, R. Frade, *Cancer Res.* **2004**, *64*, 146 – 151.

[13] J. Kos, A. Sekirnik, G. Kopitar, N. Cimerman, K. Kayser, A. Stremmer, W. Fiehn, B. Werle, *Br. J. Cancer* **2001**, *85*, 1193 – 1200.

[14] J. A. Gormley, S. M. Hegarty, A. O'Grady, M. R. Stevenson, R. E. Burden, H. L. Barrett, C. J. Scott, J. A. Johnston, R. H. Wilson, E. W. Kay, P. G. Johnston, S. A. Olwill, *Br. J. Cancer* **2011**, *105*, 1487 – 1494.

[15] S. Y. Ardebili, I. Zajc, B. Gole, B. Campos, C. Herold-Mende, S. Drmota, T. T. Lah, *Radiol. Oncol.* **2011**, *45*, 102 – 115.

[16] P. Garnero, O. Borel, I. Byrjalsen, M. Ferreras, F. H. Drake, M. S. McQueney, N. T. Foged, P. D. Delmas, J. M. Delaisse, *J. Biol. Chem.* **1998**, *273*, 32347 – 32352.

[17] D. Brömme, K. Okamoto, B. B. Wang, S. Biroc, *J. Biol. Chem.* **1996**, *271*, 2126 – 2132.

[18] K. D. Brubaker, R. L. Vessella, L. D. True, R. Thomas, E. Corey, *J. Bone Miner. Res.* **2003**, *18*, 222 – 230.

[19] I. Rapa, M. Volante, S. Cappia, R. Rosas, G. V. Scagliotti, M. Papotti, *Am. J. Clin. Pathol.* **2006**, *125*, 847 – 854.

[20] C. G. Kleer, N. Bloushtain-Qimron, Y. H. Chen, D. Carrasco, M. Hu, J. Yao, S. K. Kraeft, L. C. Collins, M. S. Sabel, P. Argani, R. Gelman, S. J. Schnitt, I. E. Krop, K. Polyak, *Clin. Cancer Res.* **2008**, *14*, 5357 – 5367.

[21] a) B. F. Sloane, M. Sameni, I. Podgorski, D. Cavallo-Medved, K. Moin, *Annu. Rev. Pharmacol. Toxicol.* **2006**, *46*, 301 – 315; b) G. Blum, *Curr. Opin. Drug Discovery Dev.* **2008**, *11*, 708 – 716; c) T. E. McCann, N. Kosaka, B. Turkbey, M. Mitsunaga, P. L. Choyke, H. Kobayashi, *NMR Biomed.* **2011**, *24*, 561 – 568; d) S. Serim, U. Haedke, S. H. L. Verhelst, *ChemMedChem* **2012**, *7*, 1146 – 1159.

[22] C. Bremer, C. H. Tung, A. Bogdanov, R. Weissleder, *Radiology* **2002**, *222*, 814 – 818.

[23] G. Blum, G. von Degenfeld, M. J. Merchant, H. M. Blau, M. Bogyo, *Nat. Chem. Biol.* **2007**, *3*, 668 – 677.

[24] a) R. W. Mason, D. Wilcox, P. Wikstrom, E. N. Shaw, *Biochem. J.* **1989**, *257*, 125 – 129; b) M. Bogyo, S. Verhelst, V. Bellingard-Dubouchaud, S. Toba, D. Greenbaum, *Chem. Biol.* **2000**, *7*, 27 – 38.

[25] T. Quillard, K. Croce, F. A. Jaffer, R. Weissleder, P. Libby, *Thromb. Haemostasis* **2011**, *105*, 828 – 836.

[26] a) H. J. Breyholz, S. Wagner, A. Faust, B. Riemann, C. Holtke, S. Hermann, O. Schober, M. Schäfers, K. Kopka, *ChemMedChem* **2010**, *5*, 777 – 789; b) U. auf dem Keller, C. L. Bellac, Y. Li, Y. Lou, P. F. Lange, R. Ting, C. Harwig, R. Kappelhoff, S. Dedhar, M. J. Adam, T. J. Ruth, F. Benard, D. M. Perrin, C. M. Overall, *Cancer Res.* **2010**, *70*, 7562 – 7569; c) V. Hugenberg, H. J. Breyholz, B. Riemann, S. Hermann, O. Schober, M. Schäfers, U. Gangadharmath, V. Mocharla, H. Kolb, J. Walsh, W. Zhang, K. Kopka, S. Wagner, *J. Med. Chem.* **2012**, *55*, 4714 – 4727.

[27] G. Ren, G. Blum, M. Verdoes, H. Liu, S. Syed, L. E. Edgington, O. Gheysens, Z. Miao, H. Jiang, S. S. Gambhir, M. Bogyo, Z. Cheng, *PLoS One* **2011**, *6*, e28029.

[28] S. M. Ametamey, M. Honer, P. A. Schubiger, *Chem. Rev.* **2008**, *108*, 1501 – 1516.

[29] a) M. Frizler, M. Stirnberg, M. T. Sisay, M. Gütschow, *Curr. Top. Med. Chem.* **2010**, *10*, 294 – 322; b) F. F. Fleming, L. Yao, P. C. Ravikumar, L. Funk, B. C. Shook, *J. Med. Chem.* **2010**, *53*, 7902 – 7917; c) V. Turk, V. Stoka, O. Vasiljeva, M. Renko, T. Sun, B. Turk, D. Turk, *Biochim. Biophys. Acta Proteins Proteomics* **2012**, *1824*, 68 – 88.

[30] R. Löser, M. Frizler, K. Schilling, M. Gütschow, *Angew. Chem.* **2008**, *120*, 4403 – 4406; *Angew. Chem. Int. Ed.* **2008**, *47*, 4331 – 4334.

[31] a) M. Frizler, F. Lohr, N. Furtmann, J. Kläs, M. Gütschow, *J. Med. Chem.* **2011**, *54*, 396 – 400; b) M. Frizler, F. Lohr, M. Lülsdorff, M. Gütschow, *Chem. Eur. J.* **2011**, *17*, 11419 – 11423; c) M. Frizler, J. Schmitz, A.-C. Schulz-Fincke, M. Gütschow, *J. Med. Chem.* **2012**, *55*, 5982 – 5986; d) M. Frizler, M. D. Mertens, M. Gütschow, *Bioorg. Med. Chem. Lett.* **2012**, *22*, 7715 – 7718; e) P. A. Ottersbach, J. Schmitz, G. Schnakenburg, M. Gütschow, *Org. Lett.* **2013**, *15*, 448 – 451; f) X. F. Ren, H. W. Li, X. Fang, Y. Wu, L. Wang, S. Zou, *Org. Biomol. Chem.* **2013**, *11*, 1143 – 1148.

[32] a) R. Löser, J. Gut, P. J. Rosenthal, M. Frizler, M. Gütschow, K. T. Andrews, *Bioorg. Med. Chem. Lett.* **2010**, *20*, 252 – 255; b) Y. H. Loh, H. B. Shi, M. Y. Hu, S. Q. Yao, *Chem. Commun.* **2010**, *46*, 8407 – 8409; c) P. Y. Yang, M. Wang, L. Li, H. Wu, C. Y. He, S. Q. Yao, *Chem. Eur. J.* **2012**, *18*, 6528 – 6541.

[33] W. J. Middleton, *J. Org. Chem.* **1975**, *40*, 574 – 578.

[34] a) W. Wadsak, L. K. Mien, D. E. Ettlinger, H. Eidherr, D. Haeusler, K. M. Sindelar, B. K. Keppler, R. Dudczak, K. Kletter, M. Mitterhauser, *Nucl. Med. Biol.* **2007**, *34*, 1019 – 1028; b) M. R. Zhang, K. Suzuki, *Curr. Top. Med. Chem.* **2007**, *7*, 1817 – 1828.

[35] J. L. Musachio, J. Shah, V. W. Pike, *J. Labelled Compd. Radiopharm.* **2005**, *48*, 735 – 747.

[36] O. Prante, R. Tietze, C. Hocke, S. Löber, H. Hübner, T. Kuwert, P. Gmeiner, *J. Med. Chem.* **2008**, *51*, 1800 – 1810.

[37] a) H.-H. Heidtmann, U. Salge, K. Havemann, H. Kirschke, B. Wiederanders, *Oncol. Res.* **1993**, *5*, 441 – 451; b) B. Werle, W. Ebert, W. Klein, E. Spiess, *Biol. Chem. Hoppe-Seyler* **1995**, *376*, 157 – 164; c) P. Ledakis, W. T. Tester, N. Rosenberg, D. Romero-Fischmann, I. Daskal, T. T. Lah, *Clin. Cancer Res.* **1996**, *2*, 561 – 568; d) E. Krepela, *Neoplasma* **2001**, *48*, 332 – 349; e) B. Werle, M. Kotzsch, T. T. Lah, J. Kos, D. Gabrijelcic-Geiger, E. Spiess, J. Schirren, W. Ebert, W. Fiehn, T. Luther, V. Magdolen, M. Schmitt, N. Harbeck, *Anticancer Res.* **2004**, *24*, 4147 – 4161.

[38] a) A. A. Wilson, L. Jin, A. Garcia, J. N. DaSilva, S. Houle, *Appl. Radiat. Isot.* **2001**, *54*, 203 – 208; b) R. N. Waterhouse, *Mol. Imaging Biol.* **2003**, *5*, 376 – 389.

[39] P. H. Hinderling, *Pharmacol. Rev.* **1997**, *49*, 279 – 295.

[40] a) K. N. Dalby, W. P. Jencks, *J. Chem. Soc. Perkin Trans. 2* **1997**, 1555 – 1563; b) P. A. MacFaul, A. D. Morley, J. J. Crawford, *Bioorg. Med. Chem. Lett.* **2009**, *19*, 1136 – 1138.

[41] A. Pastore, G. Federici, E. Bertini, F. Piemonte, *Clin. Chim. Acta* **2003**, *333*, 19 – 39.

[42] O. W. Griffith, A. Meister, *J. Biol. Chem.* **1979**, *254*, 7558 – 7560.

[43] O. W. Griffith, *J. Biol. Chem.* **1982**, *257*, 13704 – 13712.

[44] H. C. Palfrey, S. Leung, *Am. J. Physiol.* **1993**, *264*, C1270 – C1277.

[45] A. Gupta, S. Seifert, R. Syhre, M. Scheunemann, P. Brust, B. Johannsen, *Radiochim. Acta* **2001**, *89*, 43 – 49.

[46] J. N. Commandeur, G. J. Stijntjes, N. P. Vermeulen, *Pharmacol. Rev.* **1995**, *47*, 271 – 330.

[47] K. L. Davison, G. L. Larsen, *Xenobiotica* **1993**, *23*, 297 – 305.

[48] J. H. Lin, *Drug Metab. Dispos.* **1995**, *23*, 1008 – 1021.

[49] J. van den Hoff, *Amino Acids* **2005**, *29*, 341 – 353.

[50] H.-H. Otto, T. Schirmeister, *Chem. Rev.* **1997**, *97*, 133 – 172.

[51] R. C. Eastman, R. E. Carson, K. A. Jacobsen, S. Yechial, M. A. Channing, B. B. Dunn, J. D. Bacher, E. Baas, E. Jones, K. L. Kirk, M. A. Lesniak, J. Roth, *Diabetes* **1992**, *41*, 855 – 860.

[52] J. Schnekenburger, *Arch. Pharm.* **1969**, *302*, 822 – 827.

[53] Z. P. Li, J. van Lier, C. C. Leznoff, *Can. J. Chem.* **1999**, *77*, 138 – 145.

Received: March 27, 2013
Revised: May 22, 2013
Published online on ■■ ■■, 0000